The dynamic behaviour of the stall-regulated Nibe A wind turbine. Measurements and a model for stall-induced vibrations

Lundsager, Per; Petersen, H.; Frandsen, S.

Publication date:
1981

Document Version
Publisher's PDF, also known as Version of record

RISØ-M-2253

THE DYNAMIC BEHAVIOUR OF THE STALL-REGULATED NIBE A WIND TURBINE. MEASUREMENTS AND A MODEL FOR STALL-INDUCED VIBRATIONS

P. Lundsager, H. Petersen, and S. Frandsen

Abstract. The report is in two parts. In the first part the preliminary measurement system used is described, and a survey of the measurements made until the end of March 1980 is given. Results are presented concerned with the measurements of tower eigenfrequencies, eigenfrequencies of the stationary rotor and the characteristics of both flapwise and edgewise bending moments. The findings are compared with the design assumptions, and the agreement is found to be good. In the second part the possible occurrence of stall-induced blade vibrations is investigated. Vibrations with first flapping eigenfrequency are reported and a one degree of freedom model with velocity-dependent load is presented. Calculated results are shown with agree reasonably well with measured characteristics. A possible modification of the stay system is suggested.

EDB discriptors: COMPUTER CALCULATIONS; DYNAMIC LOADS; EIGENFREQUENCY; FATIGUE; FREQUENCY RESPONSE TESTING; MECHANICAL VIBRATIONS; ROTORS, STRESSES; TURBINE BLADES, WIND TURBINES.

UDC 621.548 : 534

November 1981

Risø National Laboratory, DK 4000 Roskilde, Denmark

The work described in this report was made under contract with the wind power program of the ministry of energy and the electric utilities of Denmark

ISBN 87-550-0815-1
ISSN 0418-6435

Risø Repro 1982

CONTENTS

Page

PART I: PRELIMINARY RESULTS FROM BLADE LOAD MEASUREMENTS FOR THE NIBE A WIND TURBINE

Paper presented at 4th Expert Meeting "Rotor Blade Technology with special respect to Fatique Design Problems" in Stockholm April 21th and 22th, 1980.

Preliminary Results from Blade Load Measurements for the Nibe "A" Wind Turbine

by
Per Lundsager and Helge Petersen
Risø National Laboratory, Denmark

The Nibe "A" wind turbine is one of the two wind turbines erected by the

Wind Power Program of the Ministry of Commerce
and the Electric Utilities of Denmark

near the town Nibe in Jutland, Denmark.

The wind turbine has a diameter of 40 metres, a height of 45 m and is equipped with an asynchronous generator of 630 kW.

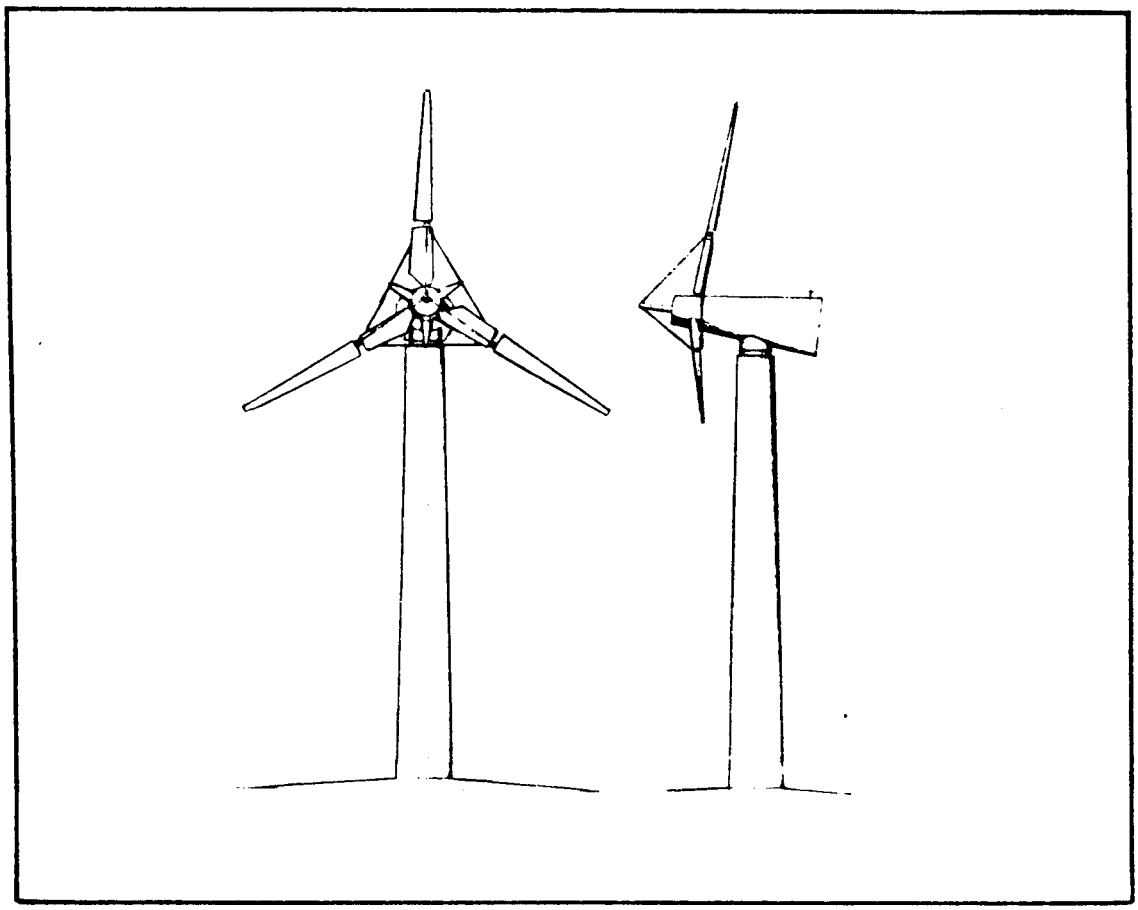

1. THE PRELIMINARY MEASUREMENT SYSTEM

The preliminary measurement system was established by connecting a number of operational parameter sensors to a six channel brush writer and an xy-plotter. A total of twelve operational parameters are available (cf. Table 1.1), the channels being connected to the brush writer six at a time through a patch panel located adjacent to the writer in the bottom of the tower of the turbine. In addition all strain gauge rotor channels are available at the patch panel three at a time through slip rings on the rotor shaft. Changes of rotor channel combinations are made by changing cable connections in the rotor hub. A diagram of the total system is shown in Fig. 1.1. Drop resistances on current signals are indicated.

Channel	Sensor	Range volt	Range Phys.	Conversion
3	Wind Speed at 58 m	0-3.0		9.3v+0 m/s
4	Rel. Wind Direction	0-2.5	-180/+180 deg	144v-180 deg
5	Blade pitch angle	0-2.2	-20/+15 deg	16v-20 deg
6	Rotor shaft torque	0-4.5	0/180 kNm	40v+0 kNm
7	RPM Generator	0-8.5	0/2250 vpm	180v+0 vpm
9	Force a. Pitch regulation	0-4.4	0/91 bar	36.4v+0 bar
10	Force b. Pitch regulation	0-4.4	0/91 bar	36.4v+0 bar
11	Nacelle position	0-4.4	-180/180 deg	162v-180 deg
12	Active power	0-2.0	-120/1200 kW	660v-120 kW
13	Reactive power	0-5.0	0/500 kVar	100v+0 kVar
14	Current	0-2.0	0/40 Amp	20v+0 Amp
15	Voltage	0-5.0	0/25 kV	5v+o kV
1	Rotor channel 1	-	-	-
16	Rotor channel 2	-	-	-
2	Rotor channel 3	-	-	-
NS	Acc NS tower top	0-1.0	0/2.45 m/s^2	2.45v+0 m/s^2
WE	Acc WE tower top	0-1.0	0/2.45 m/s^2	2.45v+0 m/s^2

Table 1.1 List of sensors

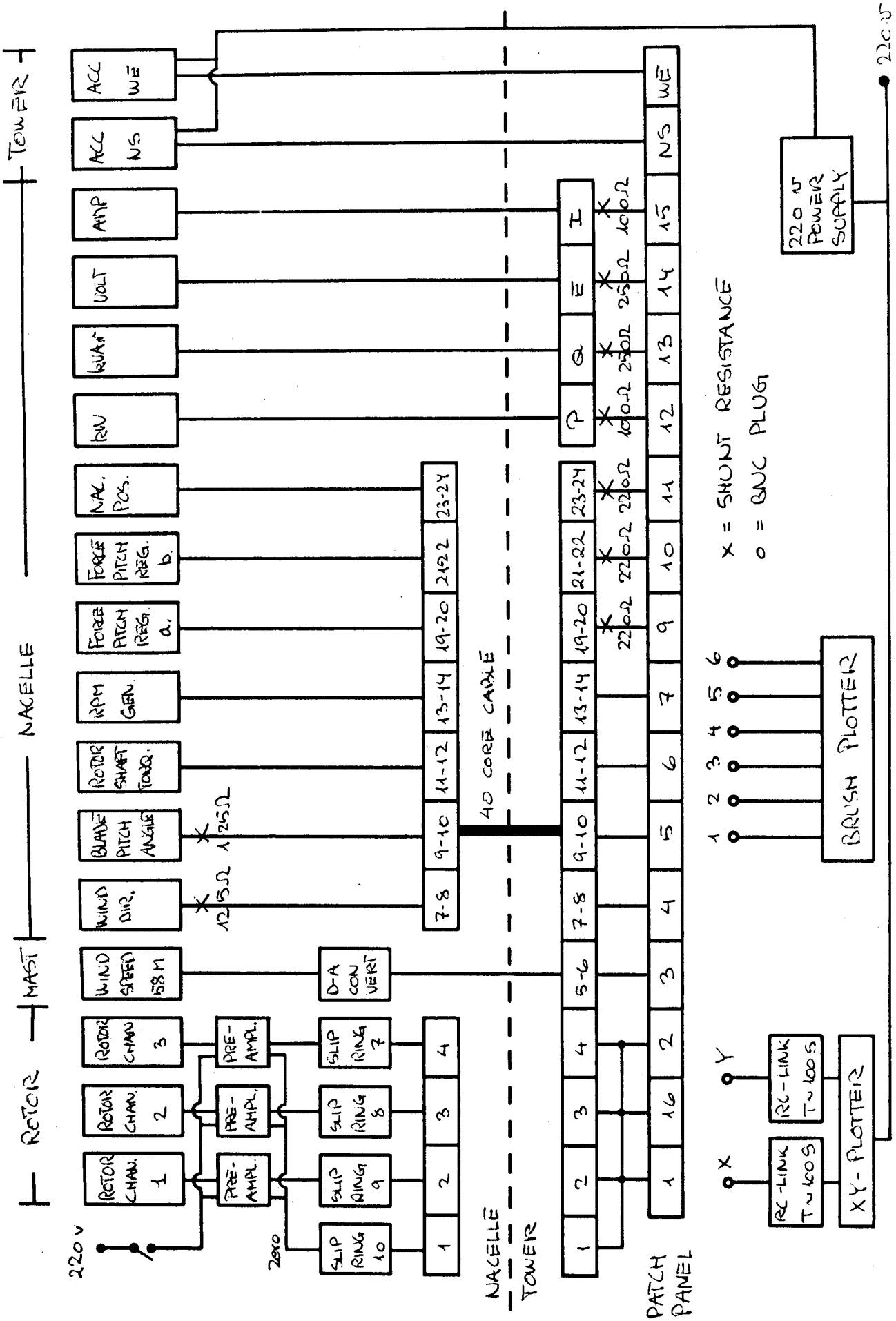
ROTOR
MAST
NACELLE
TOWER
ACC WE
ACC NS
AMP
VOLT
kWatt
RW
NAC. POS.
FORCE PITCH REG. b.
FORCE PITCH REG. a.
RPM GEN.
ROTOR SHAFT TORQ.
BLADE PITCH ANGLE
WIND DIR.
WIND SPEED 58 m
ROTOR CHAN. 3
ROTOR CHAN. 2
ROTOR CHAN. 1
PRE-AMPL.
PRE-AMPL.
PRE-AMPL.
SLIP RING 7
SLIP RING 8
SLIP RING 9
SLIP RING 10
D-A CONVERT
220 V
2000
125Ω
125Ω
40 CORE CABLE
NACELLE
TOWER
PATCH PANEL
WE
NS
I
E
Q
P
15
14
13
12
11
10
9
7
6
5
4
3
2
16
1
23-24
21-22
19-20
13-14
11-12
9-10
7-8
5-6
4
3
2
1
100Ω
250Ω
250Ω
100Ω
22kΩ
22kΩ
22kΩ
22kΩ
X = SHUNT RESISTANCE
o = BNC PLUG
1 2 3 4 5 6
BRUSH PLOTTER
220 V POWER SUPPLY
220 V
X
Y
RC-LINK TV 1005
RC-LINK TV 1005
XY-PLOTTER

Figure 1.1

Fig. 1.2 shows the rotor channels available. Sections numbered A1 to A4 are sections on mod A blades instrumented for measuring bending moments (indicated by S) or strains (indicated by T).

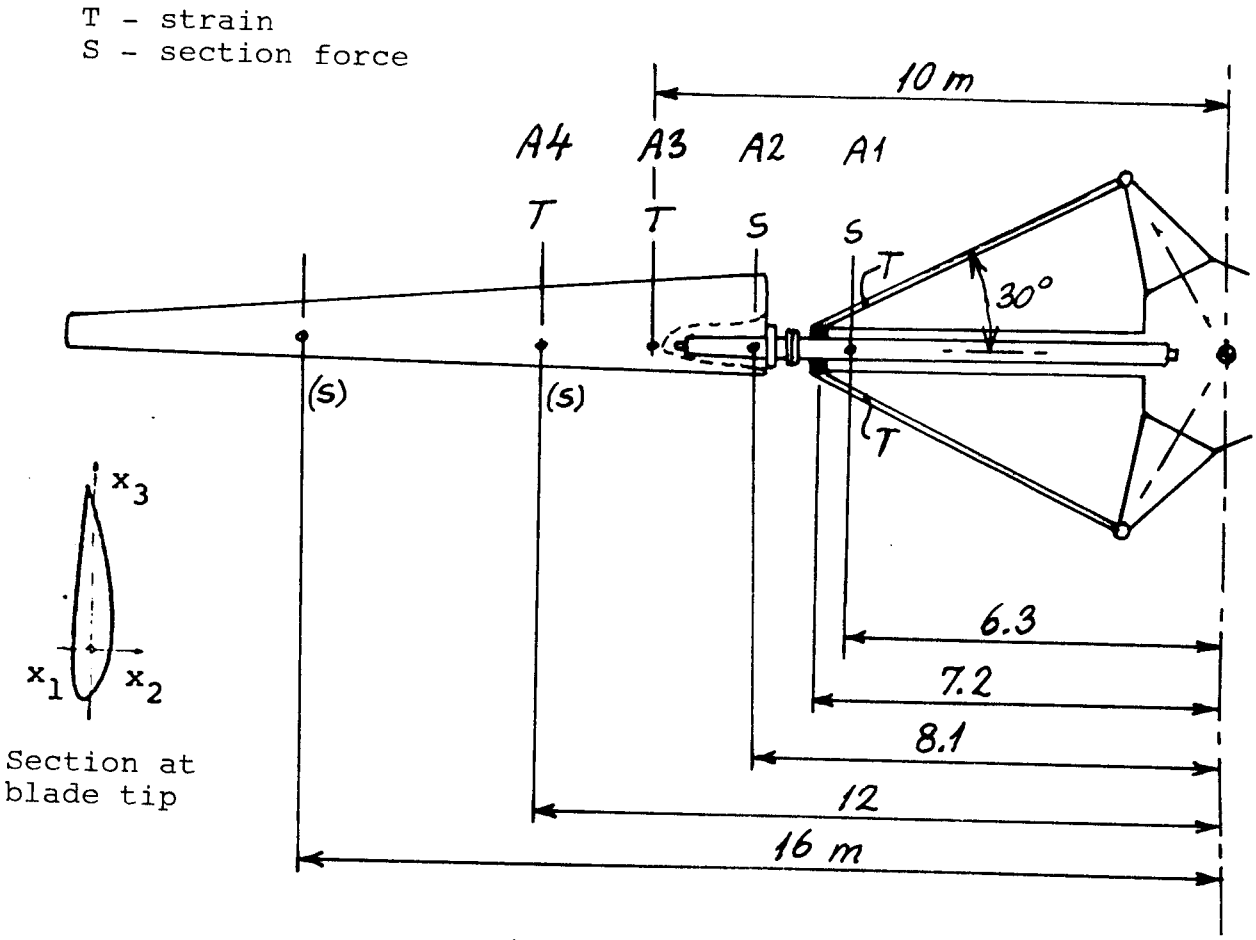

Figure 1.2

The xy-plotter is intended to give a preliminary power curve and is therefore usually permanently coupled to the wind speed and electric power channels in a mode where it plots a point every half minute. In order to simulate time-averaging in a simple manner the channels are connected to the plotter through RC-links having a time constant of approx. 100 s. Thus, excessive scatter of the points is avoided. Due to the voltage divider effects of the RC-links the plotter had to be calibrated by known voltages.

The Brush writer sentivities have been calibrated by applying known voltages. Otherwise the operational parameter signals have not been calibrated in this context; instead the calibration constants given by the operators of the turbine have been adopted in the determination of conversion factors for the preliminary measurement system. Conversion factors for the rotor channels are based on laboratory tests (ref. 1.1) conducted as part of the measurement program described in ref. 1.2. The accuracy of the results based on strip chart readings is estimated to be 5-15%. The Brush writer is able to resolve frequencies correctly up to at least 10-20 Hz.

The measurement procedures are very simple: Reconnecting channels to the brush writer using the patch panel including resetting of zero and sensitivities on the writer is accomplished in a few minutes. Reconnecting the rotor channels in the hub takes less than 30 minutes including readjustment of zero settings of the strain gauge preamplifiers. Coordination of the measurements with the operation of the turbine is performed by telephone contact with the people operating the turbine from the nacelle.

For the operational parameter signals zero voltage corresponds to a known absolute value, so that interpreting the resulting curves poses no problems. This is not the case for the rotor channels, as described in detail in refs. 1.3 and 1.4. In this presentation the rotor channel signals are referred to a zero that is obtained as the average of the max and min values of the signal during a slow revolution at the start of the turbine.

2. SURVEY OF MEASUREMENTS

Following the installation and running-in of the system four campaigns have been made as per primo April 1980. The measurement system has been used by Risø National Laboratory and by the Deparment of Fluid Mechanics of the Technical University Denmark, ref. 2.1. Some results from ref. 2.1 are included in this presentation.

In Table 2.1 the campaigns are listed and their primary aims are indicated. The rotor channel combinations available are also indicated. During each campaign a variety of operational parameters were recorded partly as aids in the commissioning of the turbine and partly as preliminary checks on the calculations of the response of the turbine. Table 2.2 shows the rotor channel combinations.

The results and conclusions in this presentation are based on records made during these four campaigns.

Campaign No	Date	Rotor Channel combination	Purpose
1	30.1.80	1	First indication of out-of-plane blade loads
2	13.2.80	1	Check of blade pitch regulation - - tower resonance
3	27-28.2.80	1	Investigation of blade pitch angle influence on blade loads and power production (ref.2.1)
5	5-6.3.80	2-4	Investigation of blade loads.

Table 2.1 List of campaigns Jan.-Mar. 1980.

Rotor channel combination	Rotor channels available
1	Out-of-plane bending moments at station A2 for all 3 blades
2	Out-of plane bending moments at station A1 for 2 blades. Force in one in-plane stay.
3	In-plane bending moments at station A1 for all 3 blades
4	In-plane bending moment for 1 blade. Forces in adjacent in-plane stays

Table 2.2 Rotor channels available

3. RESULTS

The results given in this section are recorded by the instrumentiation shown in Fig. 1.1. In Section 3.2 some results are shown, that have been obtained by means of an FFT analyzer plugged in on the patch panel. The analyzer is a Hewlett Packard 3721A that performs an actual analysis in a chosen period of time, extracting all frequencies simultaneously.

3.1. Location of sensors on the rotor.

Figure 3.1 shows the root of the outer blade and the trunnion on which it is mounted. The trunnion is shown in Fig. 3.2 together with the blade shaft. The shaft is supported by a bearing, mounted in a bearing house at the end of a tube and supported by two struts in the rotor plane and one strut out-of-plane. The figure shows the instrumented sections for which results are shown in the following sections. The strain gauges in Section A of Fig. 3.2 give flapwise bending moments used in Sections 3.3 and 3.4 of this paper. The strain gauges in Section B give flapwise bending moments used in Section 3.4 as well as chordwise bending moments shown in Section 3.5 of this paper. The struts are also equipped with strain gauges giving the tensile forces used in Section 3.5.

3.2 Determination of the tower eigenfrequency

The tower eigenfrequency has been determined by recording accelerations of the wind-induced vibrations of the tower top as well as by recording the accelerations during the upstart of the mill and identifying the resonance point.

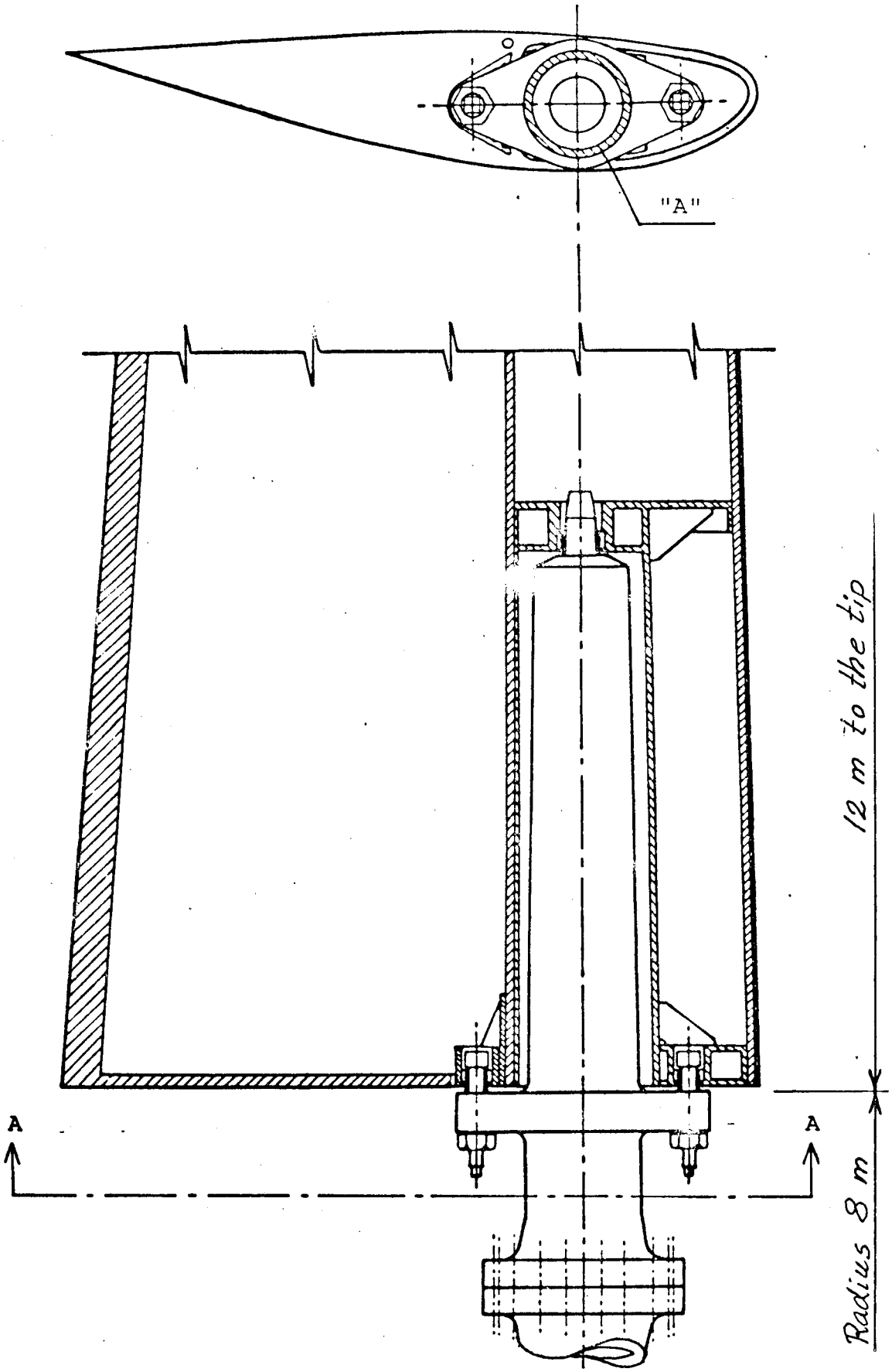

The glass-fibre wing mounted on the trunnion

Figure 3.1

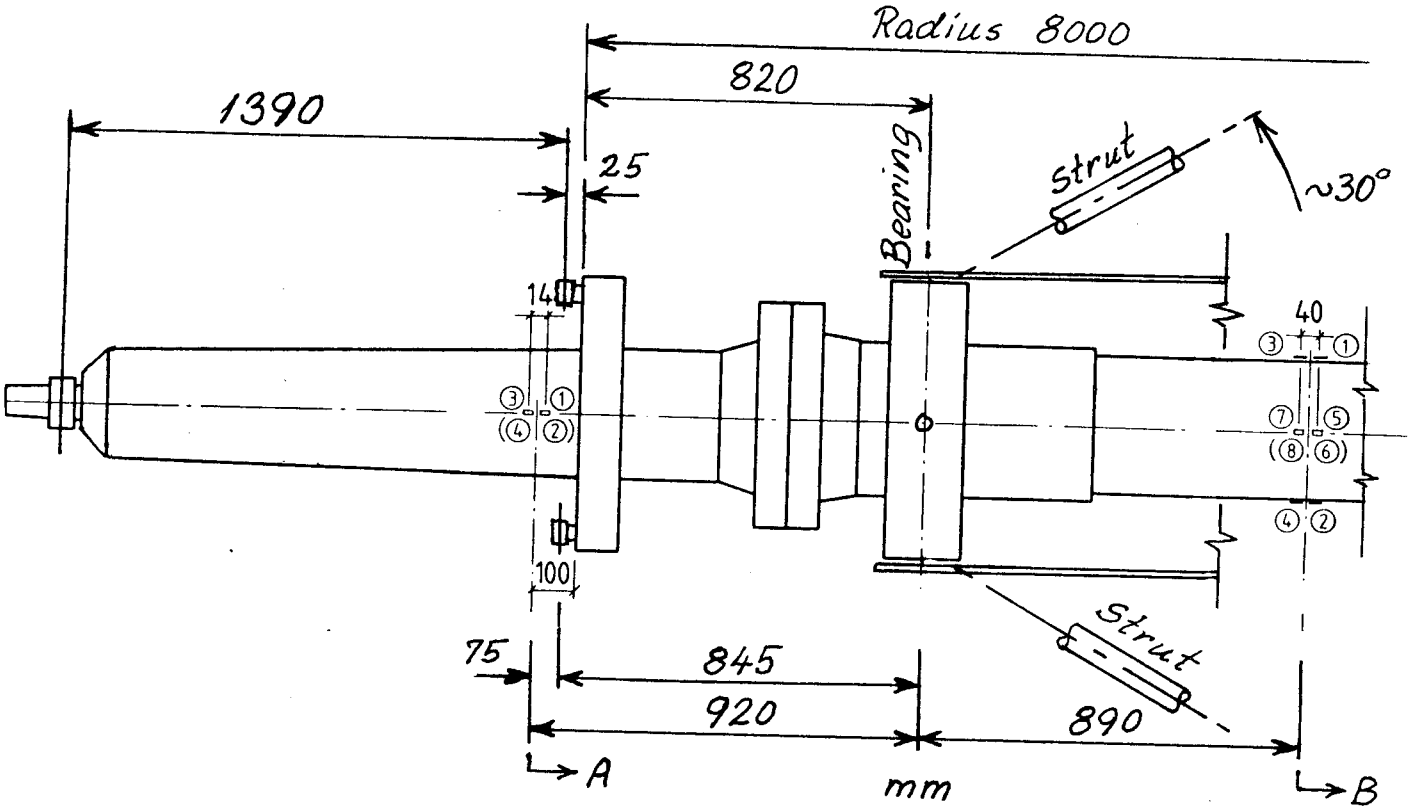

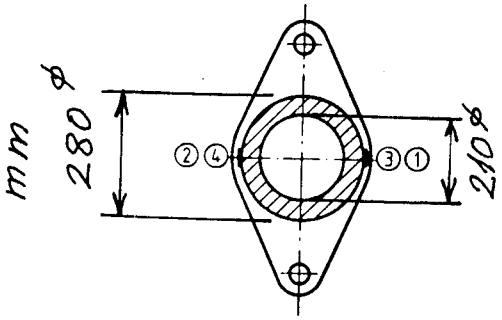

Section A
Trunnion

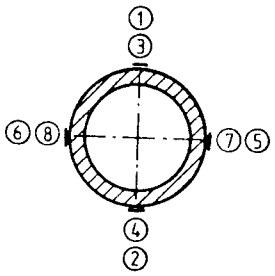

Section B
Shaft

Figure 3.2

Figure 3.3 shows time tracks of both north-south (NS) and west-east (WE) acceleration components recorded with the stopped rotor. Thus the vibrations are wind induced, and by measuring the time between tops as indicated in the figure, frequencies of 1.29 Hz and 1.34 Hz are found for the NS and WE directions, respectively.

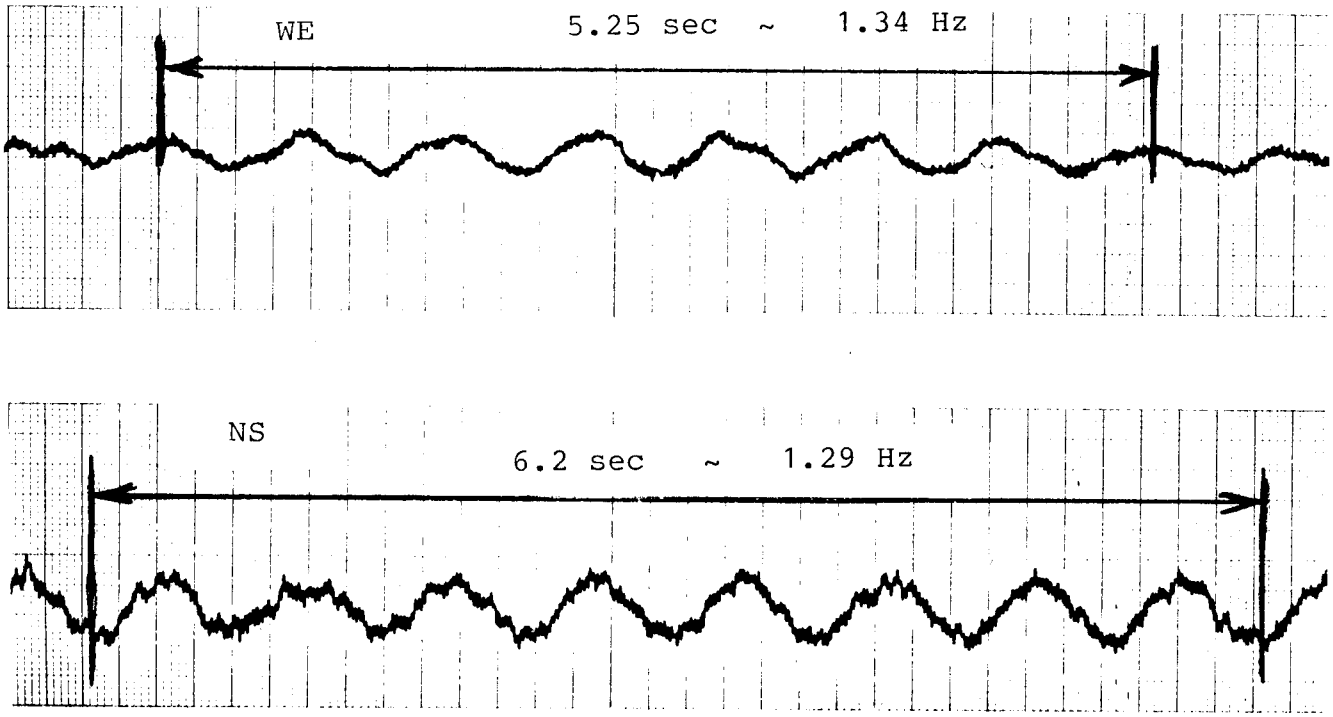

Figure 3.3

Figure 3.4 shows corresponding time tracks during a start-stop sequence. As indicated in the figure a resonance occurs at 1215 RPM on the generator shaft, corresponding to 27 RPM on the rotor shaft or 0.45 Hz. At this speed the blade passage frequency is $3 \cdot 0.45 = 1.35$ Hz.

Figure 3.5 shows the calculated values as given by the tower designer in October 1978. The calculated value 1.28 Hz is confirmed by the measurements, considering the accuracy level of this preliminary instrumentation. The signal level of the accelerometers ($\sim \pm 0.1$ V) was too small for the FFT analyzer, and therefore the eigenfrequency could not be determined by the frequency analyzer which was available.

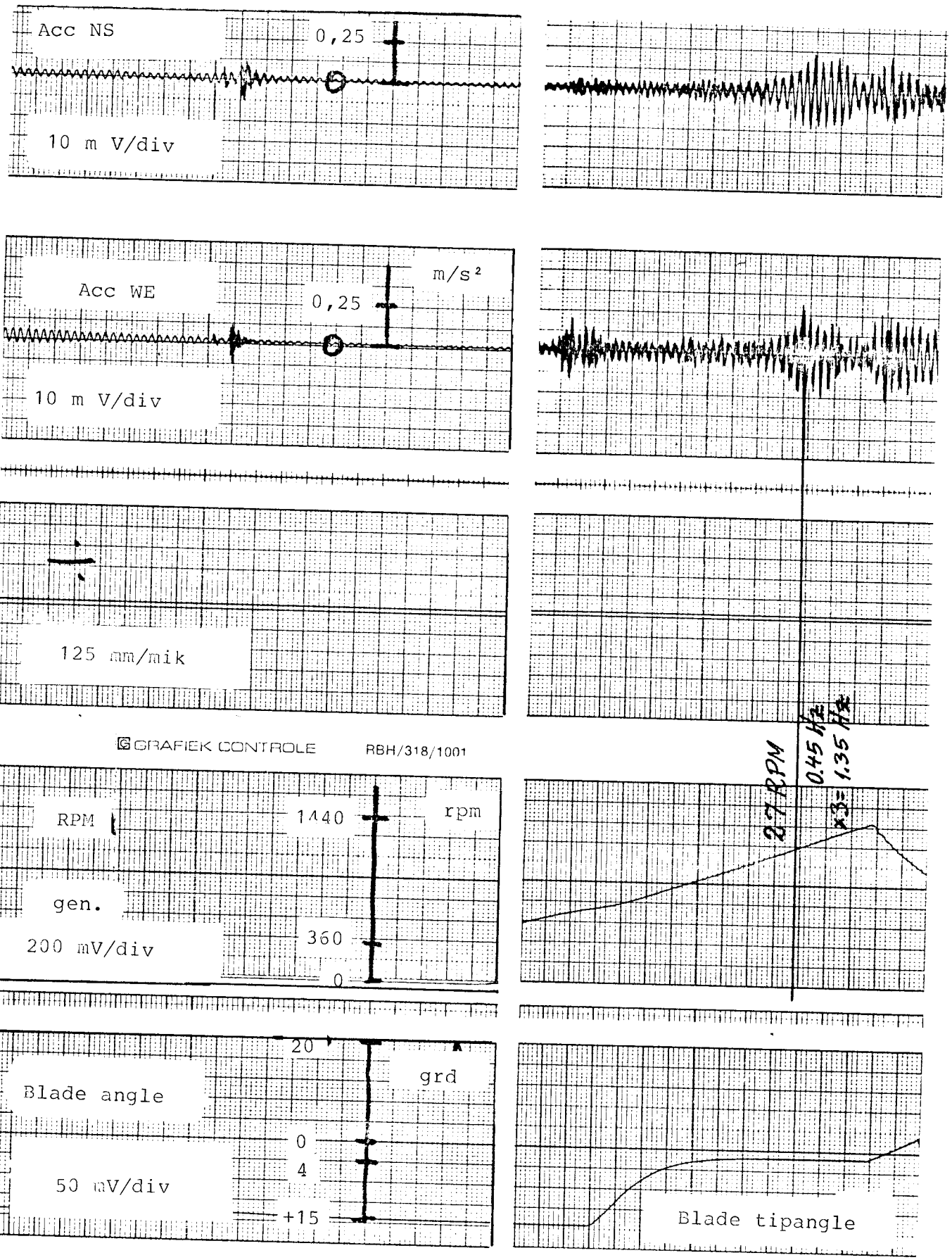
Acc NS
0,25
10 m V/div
Acc WE
m/s²
0,25
10 m V/div
125 mm/mik
GRAFIEK CONTROLE
RBH/318/1001
RPM
1440
rpm
gen.
200 mV/div
360
0
27 RPM
0.45 Hz
x3= 1.35 Hz
Blade angle
20
grd
0
4
50 mV/div
+15
Blade tipangle

Figure 3.4

Mode shapes (max. amplitude = 1.000)

Mode no	1	2	3	4	5
node no	U_x	U_x	Θ_z	U_z	U_x
1	1000	-684	1000	1000	-395
2	884	-221	968	926	250
3	752	266	835	897	811
4	627	645	712	963	1000
5	508	892	599	824	831
6	398	1000	494	780	413
7	299	978	397	733	-95
8	212	856	307	681	-535
9	139	662	224	627	-788
10	80	438	148	570	-800
11	36	222	79	510	-580
12	4	28	5	438	-106
13	0	0	0	335	0
Frequencies	1,28	7,00	9,93	13,3	16,4
	bending		tor-sion		bending

Figure 3.5

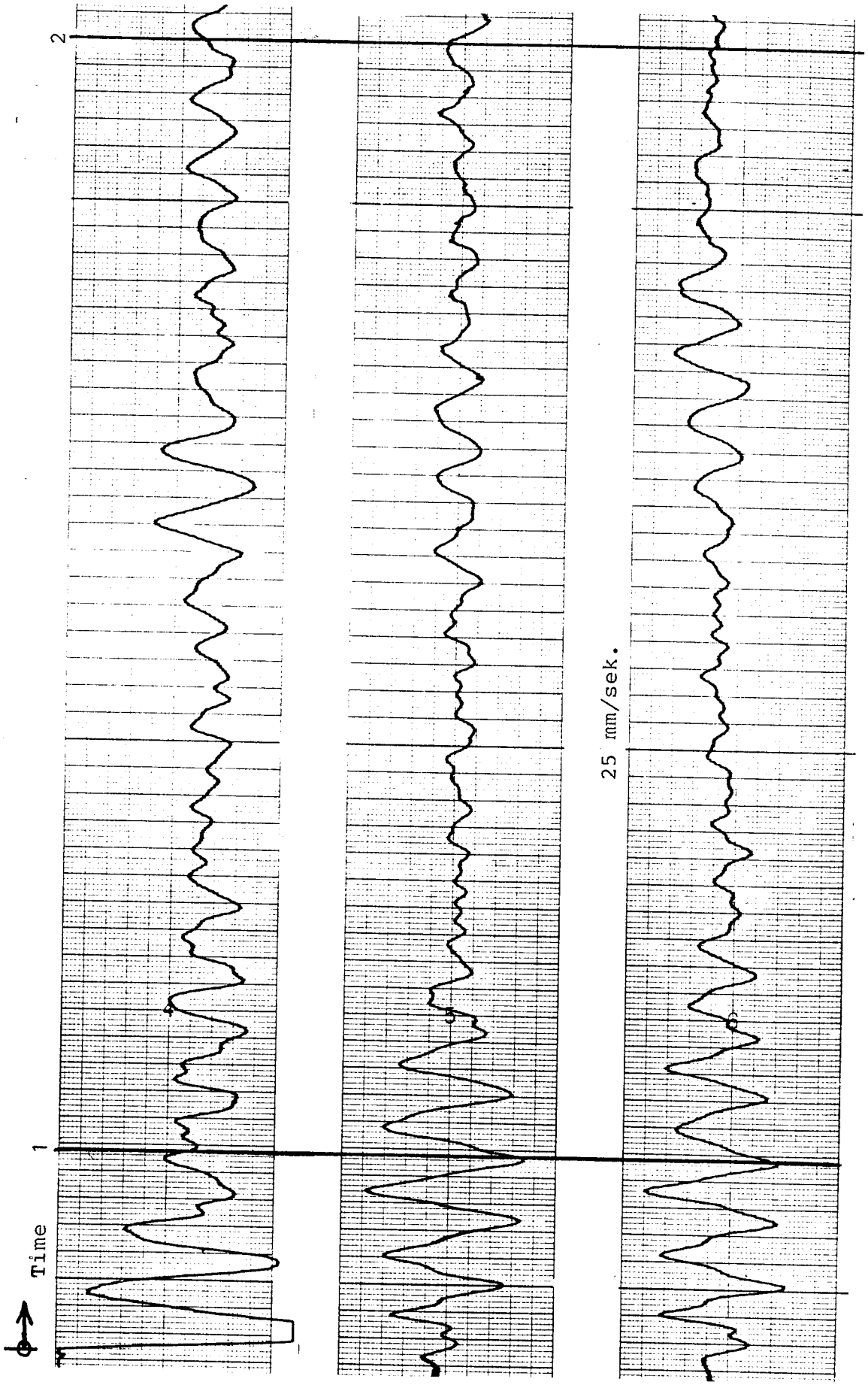

Figure 3.6

3.3 Determination of frequencies of the stationary rotor.

The frequencies were determined by a series of tests in which one of the blades was bent by pulling the tip towards the tower and releasing it. The signals from the strain gauges on the trunnion (section A in Figure 3.2) was used, and the first 10 to 15 secs were recorded and analyxed. A typical record is shown in Fig. 3.6 All three blades were successively exited blade as well as from the other blades.

Figure 3.7 shows a typical output from the FFt analyzer. In the range 1.9 - 2.3 Hz, three peaks are appearent, and a fourth one may be identifyed above 3 Hz.

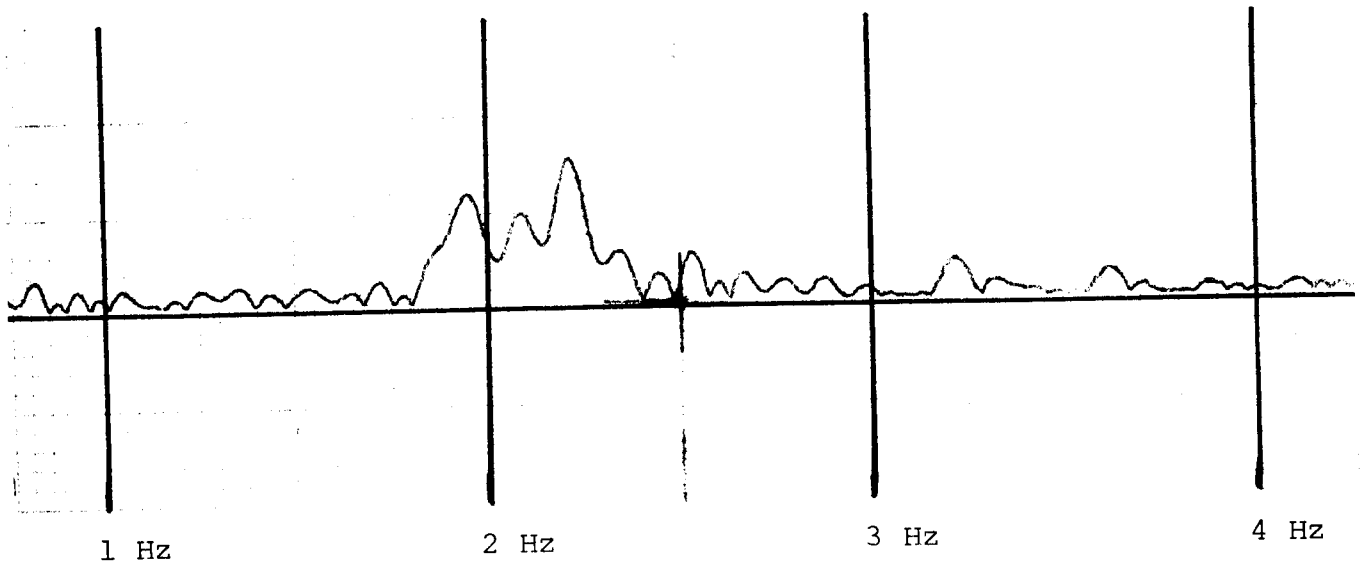

Figure 3.7

Figures 3.8a - 3.8c shows plots of calculated eigenmodes for the stationary rotor, ref. 3.1, Table 3.1 indicates the corresponding eigenfrequencies according to the latest calculations together with the eigenfrequencies determined on the basis of a series of 18 runs with the FFT analyzer.

Mode	Calculated Hz	Measured Hz
1	1.99	1.95 ± 0.04 RMS
2	1.99	2.12 ± 0.04 -
3	2.12	2.24 ± 0.03 -
4	3.33	3.44 ± 0.03 -

Table 3.1 Rotor eigenfrequencies

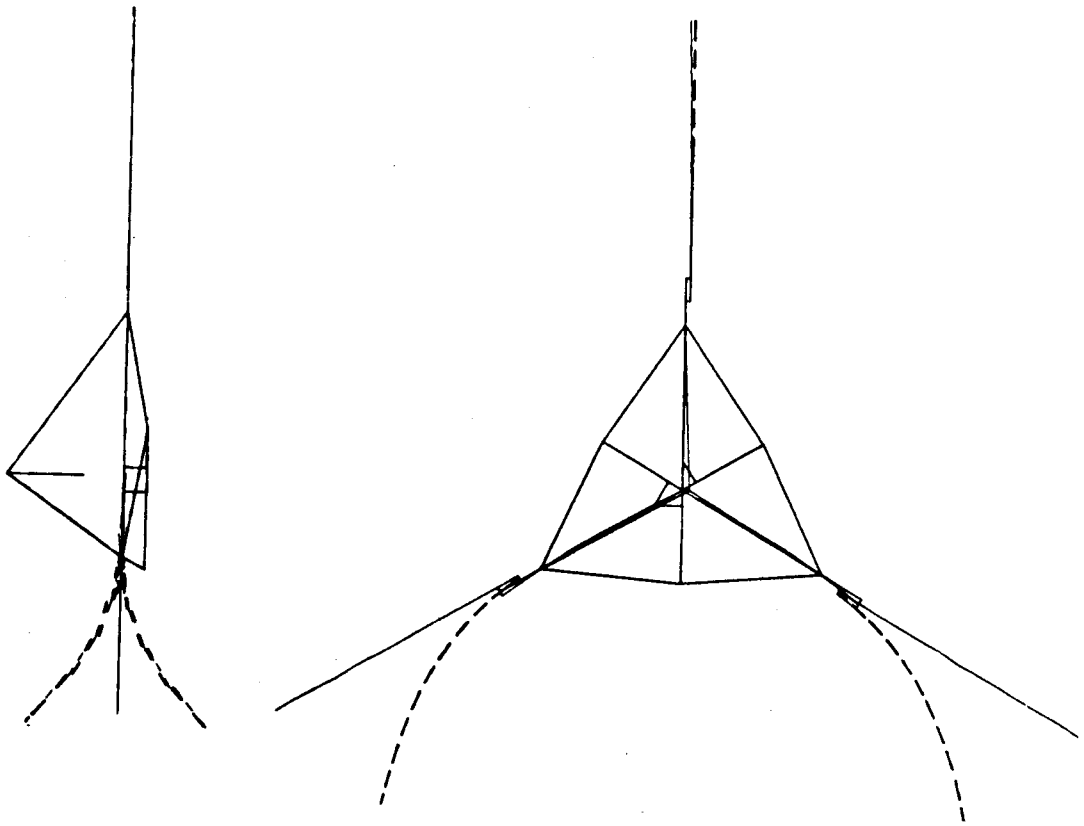

Mode 1

Figure 3.8a

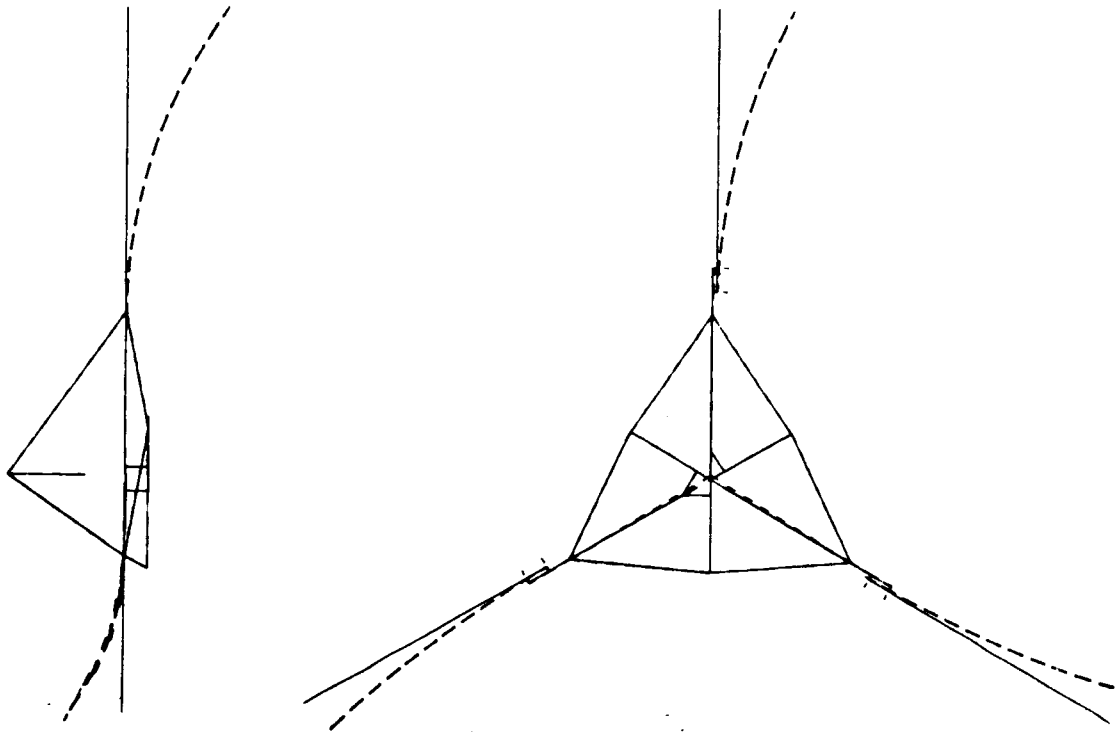

Mode 2

Figure 3.8b

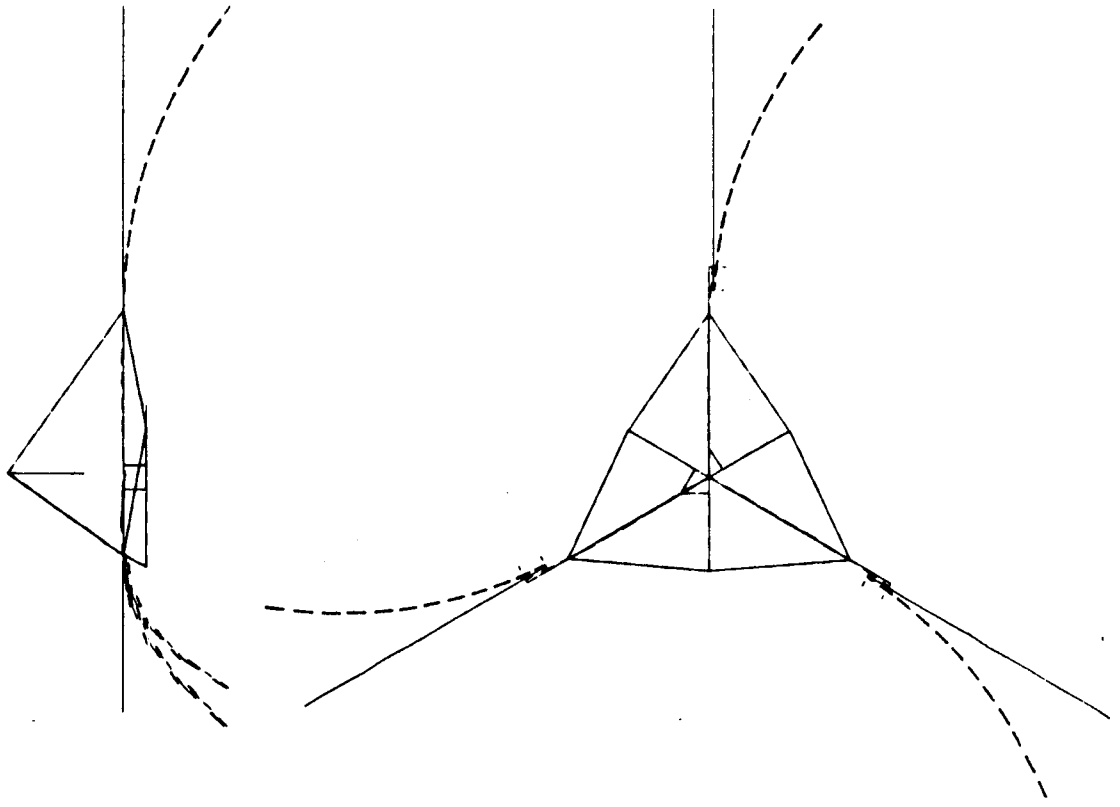

Mode 3

Figure 3.8c

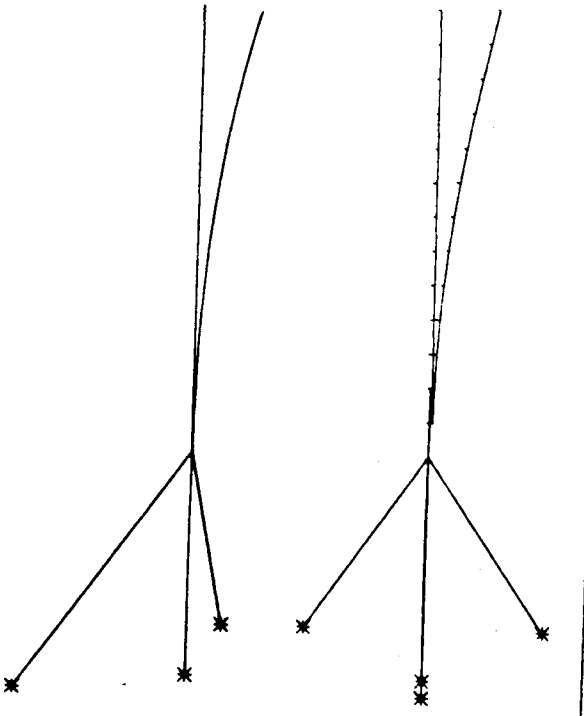

2.12 Hz

Figure 3.9a

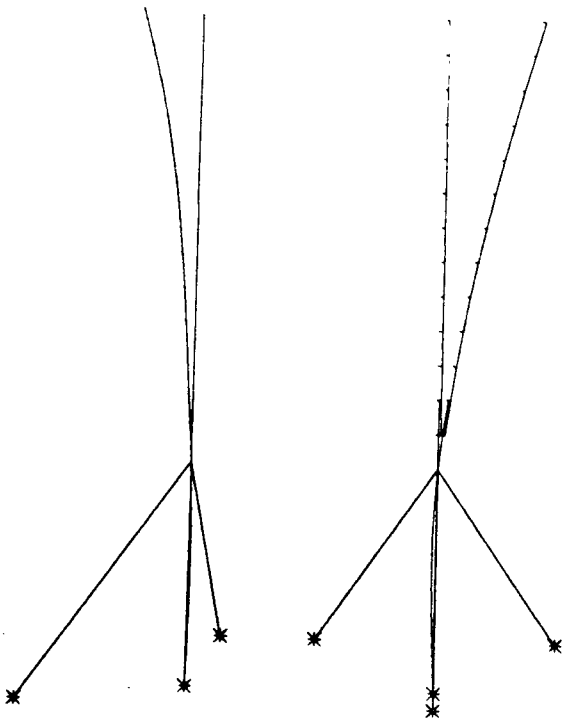

3.33 Hz

Figure 3.9b

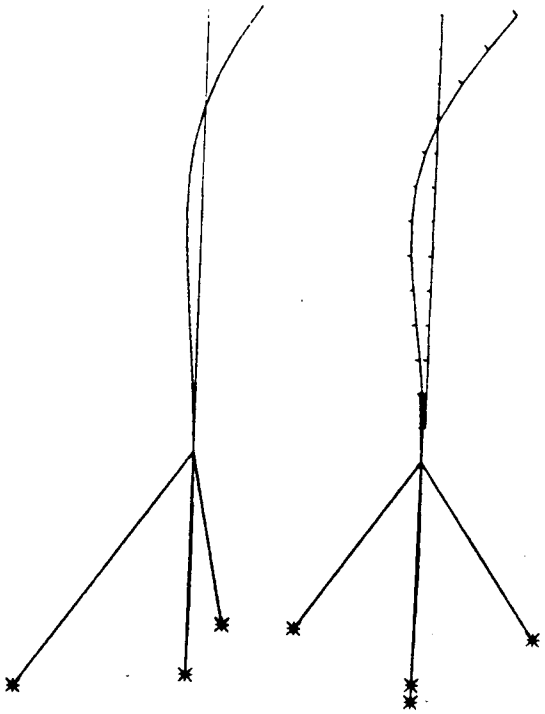

Flapwise Chordwise

6.37 Hz

Figure 3.9c

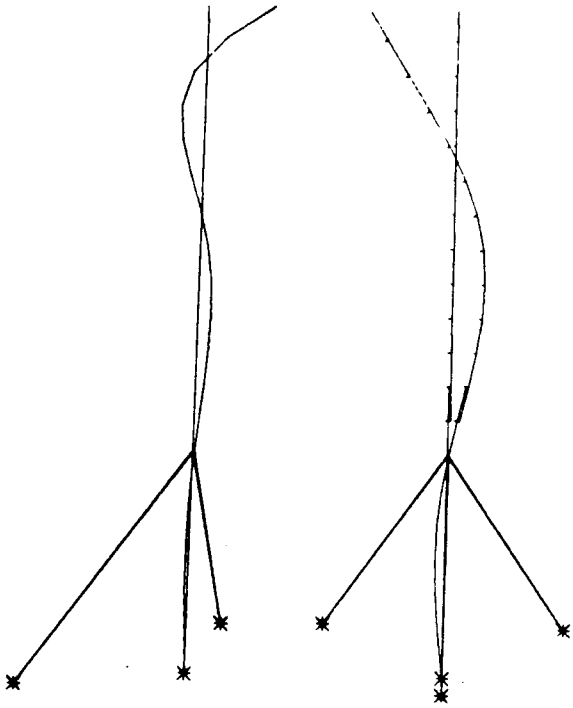

Flapwise Chordwise

12.8 Hz

Figure 3.9d

The fourth calculated eigenfrequency corresponds to the eigenmode shown in Fig. 3.9b, calculated for a single blade. The calculated frequencies are within 10% of the measured values.

The uppermost time track of Fig. 3.6 is the signal from the excited blade. At the time indicated by 1 the excited blade has a phase lag of 180 deg to the two other blades, indicating that mode 2 is predominant. After approx. 10 secs at the time indicated by 2 one blade is almost stationary while the two others are in phase, indicating that mode 1 now is predominant.

3.4. Flapwise bending moments during operation

Figure 3.10 shows records of the flapwise moments at section A, Fig. 3.2, during a normal stop at low wind speed. The dominant feature is the pronounced peak occurring when the stop sequence is initiated. From an average of approx. 44 kNm and an amplitude of approx. 23 kNm the level rises to about 95 kNm with a peak to about 140 kNm. This is due to the pitching of the blades during a normal stop gradually through maximum C_L-values to the stalled condition over a period of approx. 5 secs. This load cycle is experienced once during each stop. This occurs each time the turbine attempts to start in low wind and fails to connect to the grid.

It appears from Fig. 3.11, where a stop from approx. 13 m/s is shown that the peak of Fig. 3.10 does not occur. However, the average level of $\sim$ 95 kNm corresponds to the average level during the stop (Fig. 3.10) as the blade is already partly stalled at this condition. Therefore the peak of 130 kNm may be caused by dynamic amplification. It causes a stop from low winds to be more severe for flapwise bending than a stop from high winds.

Figure 3.12 shows records similar to those in Fig. 3.10, but taken from the flapwise sensors at section B, Fig. 3.2. Again the pronounced rise in level during the stop sequence from low speed is seen, but the peak is not so pronounced. From a level of $\sim$ 30 kNm and an amplitude of $\sim$ 24 kNm the level rises to $\sim$ 88 kNm with a maximum of $\sim$ 110 kNm.

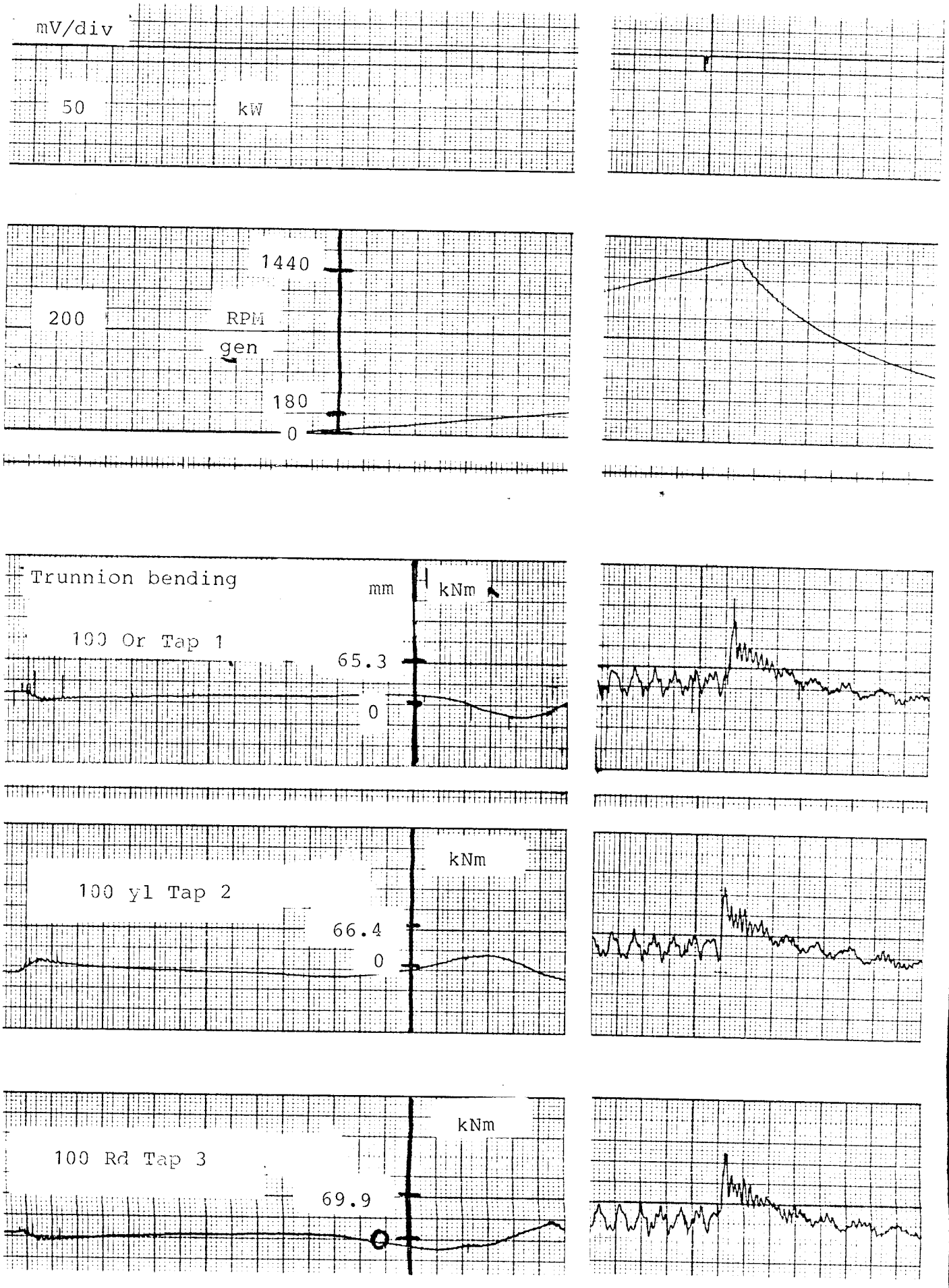
mV/div
50
kW
1440
200
RPM
gen
180
0
Trunnion bending
mm
kNm
100 Or Tap 1
65.3
0
kNm
100 yl Tap 2
66.4
0
kNm
100 Rd Tap 3
69.9

Figure 3.10

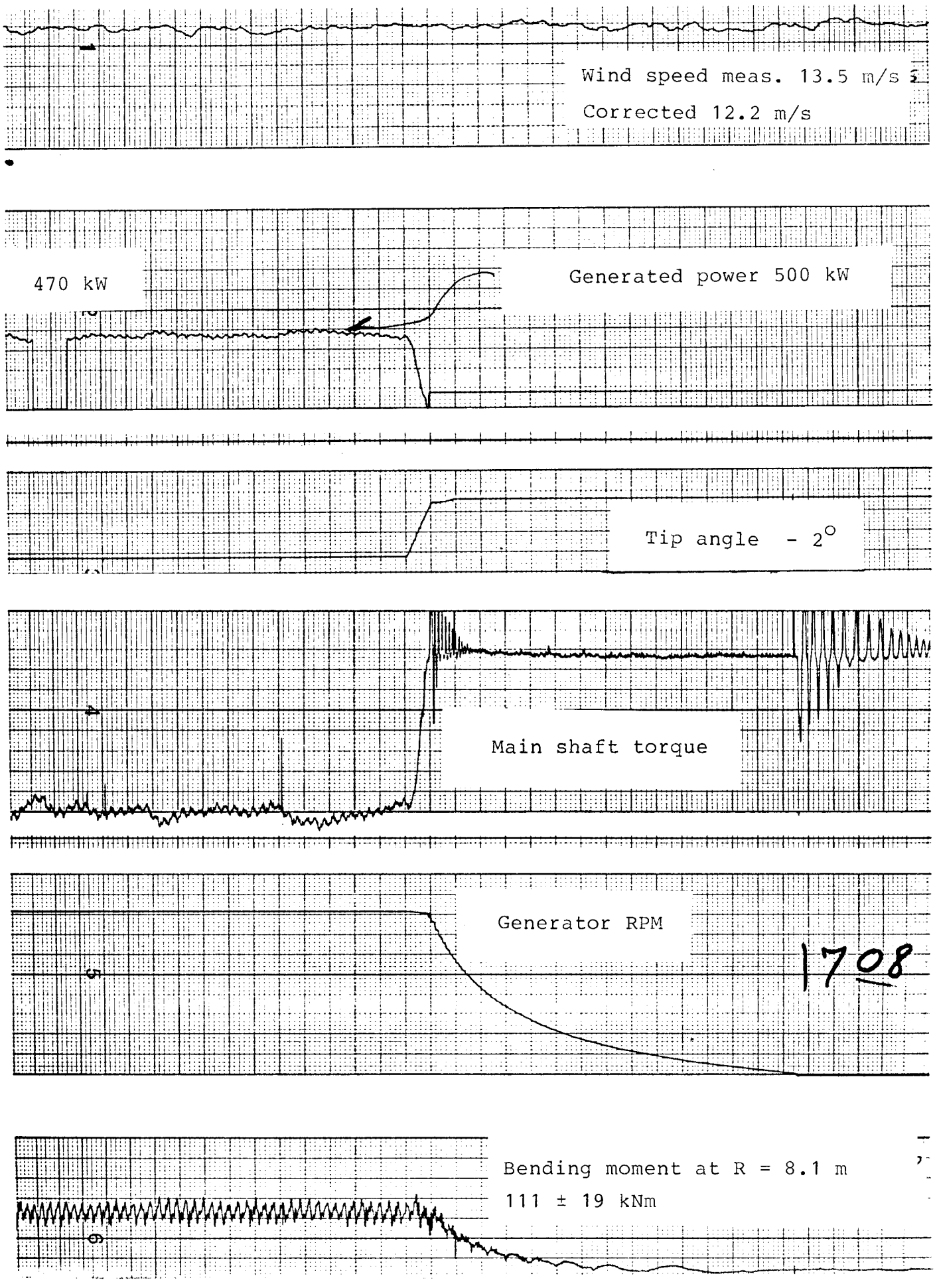
Wind speed meas. 13.5 m/s
Corrected 12.2 m/s
470 kW
Generated power 500 kW
Tip angle - 2°
Main shaft torque
Generator RPM
1708
Bending moment at R = 8.1 m
111 ± 19 kNm

Figure 3.11

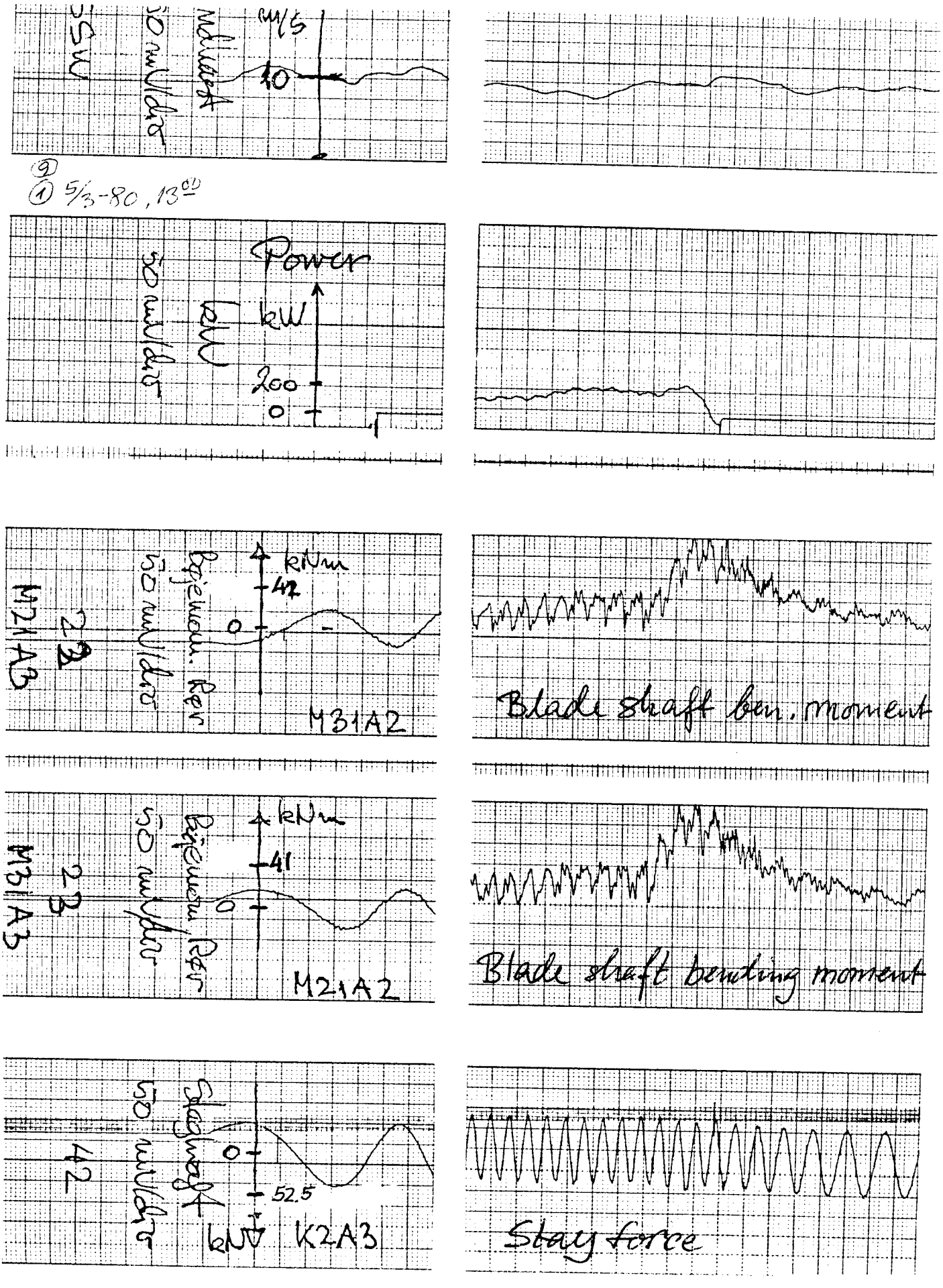
m/s
10
Power
kW
200
0
kNm
42
0
M31A2
Blade shaft ben. moment
41
M21A2
Blade shaft bending moment
52.5
K2A3
Stay force

Figure 3.12

Figure 3.13 shows the calculated flapwise bending moment distributions due to a triangular aerodynamic load (above) and the corresponding moments due to the centrifugal forces acting through the coning angle of the blade (below). By adding the centrifugal force moments at stations A and B to the levels of 95 kNm and 88 kNm, respectively, measured during stop, the moments 147 kNm and 141 kNm due to aerodynamic forces in station A and B, respectively, are obtained. This corresponds to the ratio 1.04 between the values indicated on the uppermost Fig. 3.13. Thus the computational predictions on which the design has been based are confirmed by the measurements.

Figure 3.14 shows the design spectrum calculated from wind speed statistics by the Department of Fluid Mechanics for the flapwise bending moments due to aerodynamic loads referred to zero radius. By referring the values of Figures 3.10 to 3.12 to zero radius one obtains an average of 364 kNm and an amplitude of 42 kNm. These values are within the values shown in Fig. 3.14 for $1 \cdot 10^8 - 3 \cdot 10^8$ cycles corresponding to 42% of the operational life. The peaks of Figs. 3.10 and 3.12 referred to zero radius are $\sim$ 400 kNm, which are within the values given for cycles up to $6 \cdot 10^5$, corresponding to $< 1\%$ of operational life. Thus these measurements so far do not contradict the design assumptions.

3.5. Stresses in the trunnion and the shaft

The dimensions of the steel trunnion at station A Fig. 3.13, and of the shaft in the bearing, station C, are given in Fig. 3.15. The observed peak of the bending moment during stop, Fig. 3.10, is approx. 140 kNm, and the corresponding stresses are shown in Table 3.2.

Station	Moment of inertia 10^{-4} m^4	Eccentricity m	Stress MN/m^2
A, R = 8 m	2.15	0.14	91
C, R = 7.2 m	3.10	0.16	72

Table 3.2.

At station C the stress is superposed by a tensile stress due to the centrifugal force. This tension is ~ 6 MN/m^2. The material is St. 52-3 for which the yield stress is 350-400 MN/m^2.

3.6 Driving bending moments during operation

Figure 3.16 shows the driving moment at station B, Fig. 3.2, for one blade and the forces in the two adjacent in-plane struts during a normal stop sequence. The figure shows that gravity forces are entirely dominant and that a normal stop is undramatic, although the first in-plane mode (mode 4 of Table 3.1) of $\sim$ 3.4 Hz is excited when the generator is disconnected from the grid. The peaks on the trace for the main shaft torque are due to slack in the power train (cf. ref. 2.1).

Figure 3.17 shows in more detail the traces of the driving moments in all blades at station B, the moment M31A2 being shown 2½ times enlarged compared to the two others. The traces are basically sinusoidal, but clearly superposed by the fourth mode of Table 3.1 ($\sim$ 3.4 Hz in-plane). In addition to these oscillations the trace of M31A2 shows regular cusps at the bottom of each period. One month later this cusp has developed into the abnormal trace shown in Fig. 3.18, which indicates some mechanical problem, most probably in the bearing of that particular blade (cf. Fig. 3.2).

Figure 3.19 shows the predicted in-plane moment distribution due to gravity forces when the blade is horizontal. From Fig. 3.17 the amplitude 40 kNm is read, which corresponds well to the value shown in Fig. 3.19 for the gauge on the shaft.

From Fig. 3.16 the tensile forces 10 kN and 16 kN are found in the struts pointing forward and backwards, respectively, during a short period just before stop. This corresponds to a driving force of 3 kN at radius 8 m, which again corresponds to a rotor shaft torque of 72 kNm. This agrees well with the torque 76 kNm recorded for the torque in the shaft. By comparison with the recorded electric power of 190 kW the efficiency of the power train and generator at this power is 0.75.

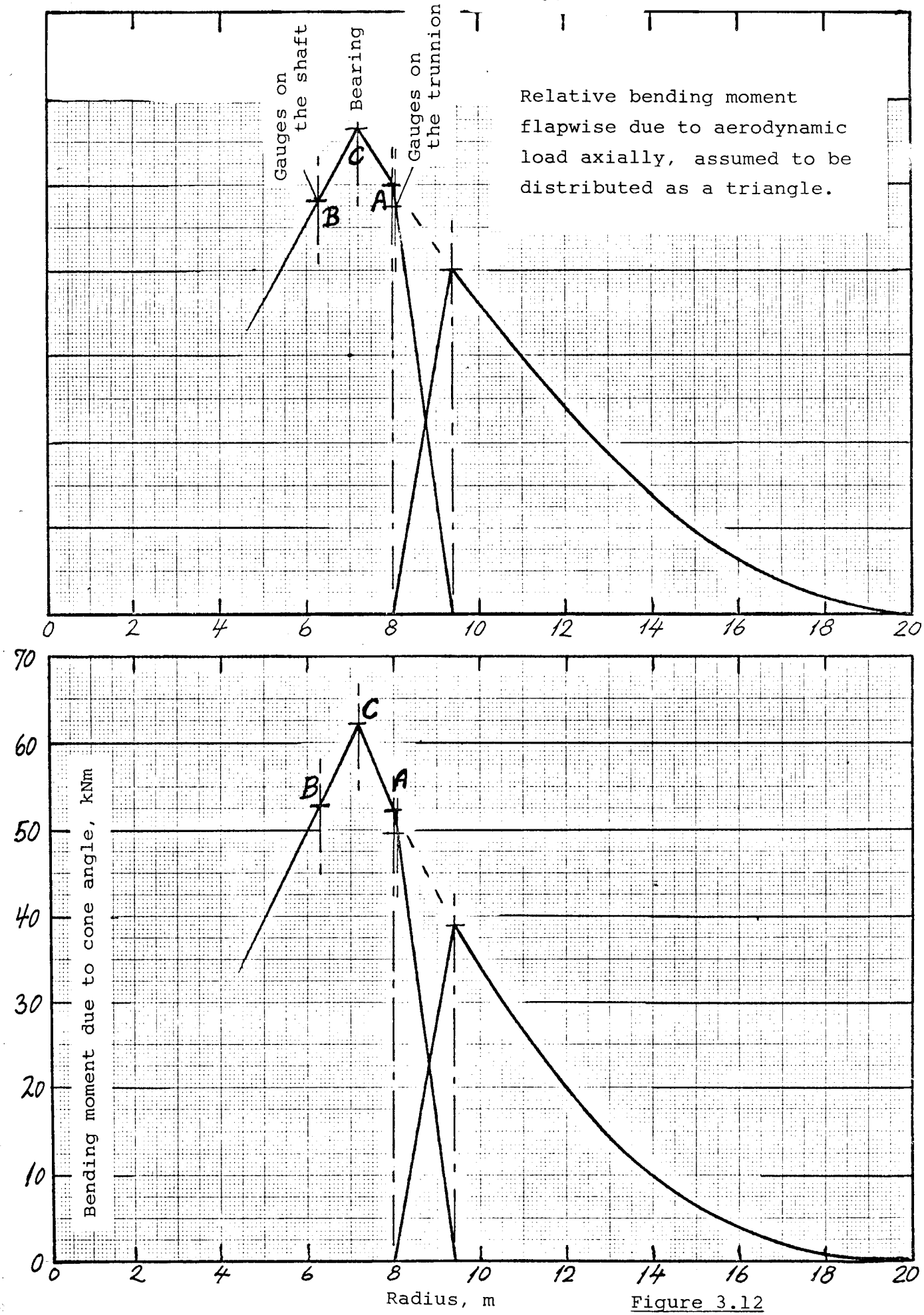
Gauges on the shaft
Bearing
Gauges on the trunnion
Relative bending moment flapwise due to aerodynamic load axially, assumed to be distributed as a triangle.
A
B
C
0
2
4
6
8
10
12
14
16
18
20
Bending moment due to cone angle, kNm
Radius, m

Figure 3.12

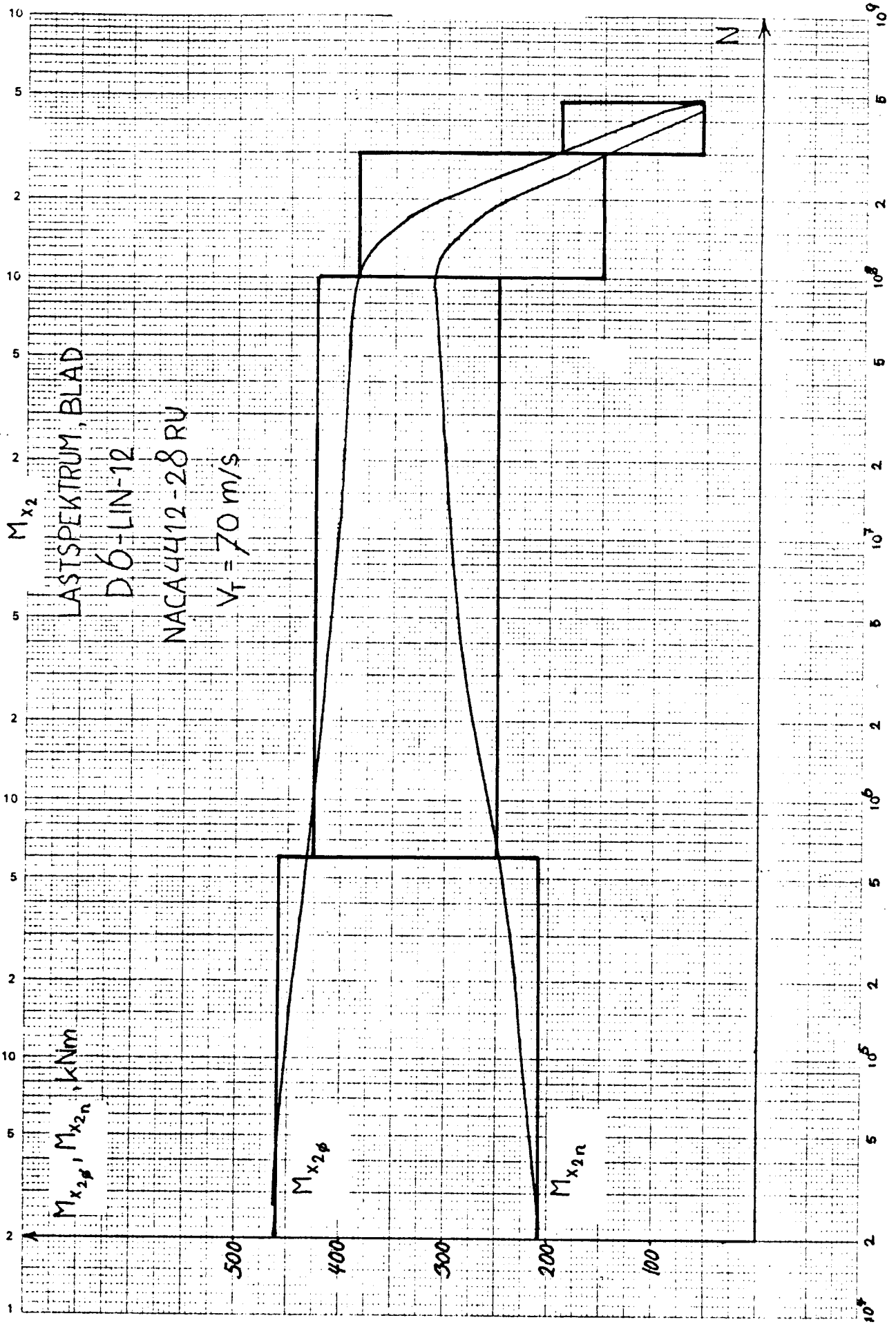
LASTSPEKTRUM, BLAD
D6-LIN-12
NACA4412-28 RU
V_T = 70 m/s
M_{x_2}
$M_{x_{2\phi}}$, $M_{x_{2n}}$, kNm
$M_{x_{2\phi}}$
$M_{x_{2n}}$
N
500
400
300
200
100

Figure 3.14

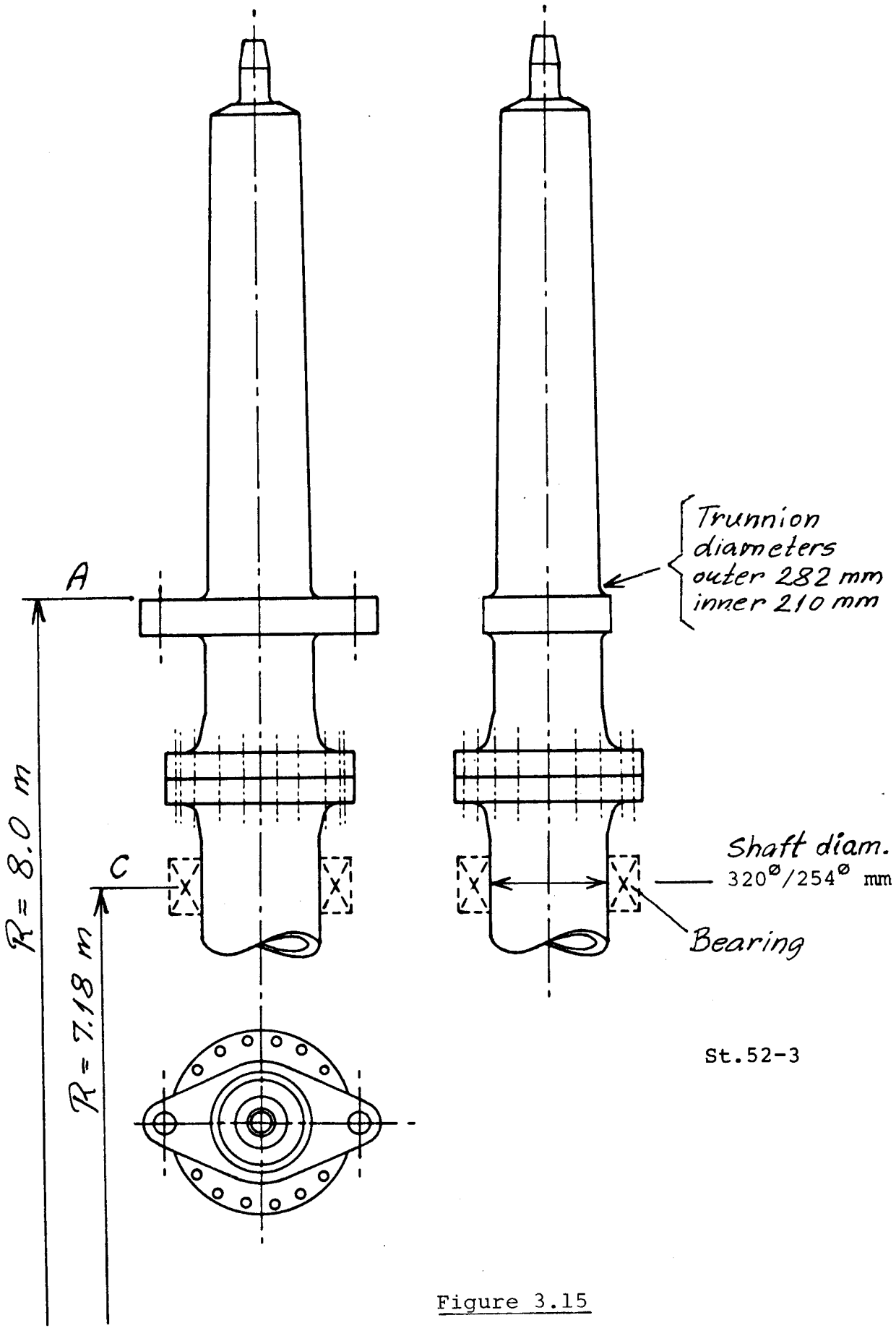
A
C
R = 8.0 m
R = 7.18 m
Trunnion
diameters
outer 282 mm
inner 210 mm
Shaft diam.
320⌀/254⌀ mm
Bearing
St.52-3

Figure 3.15

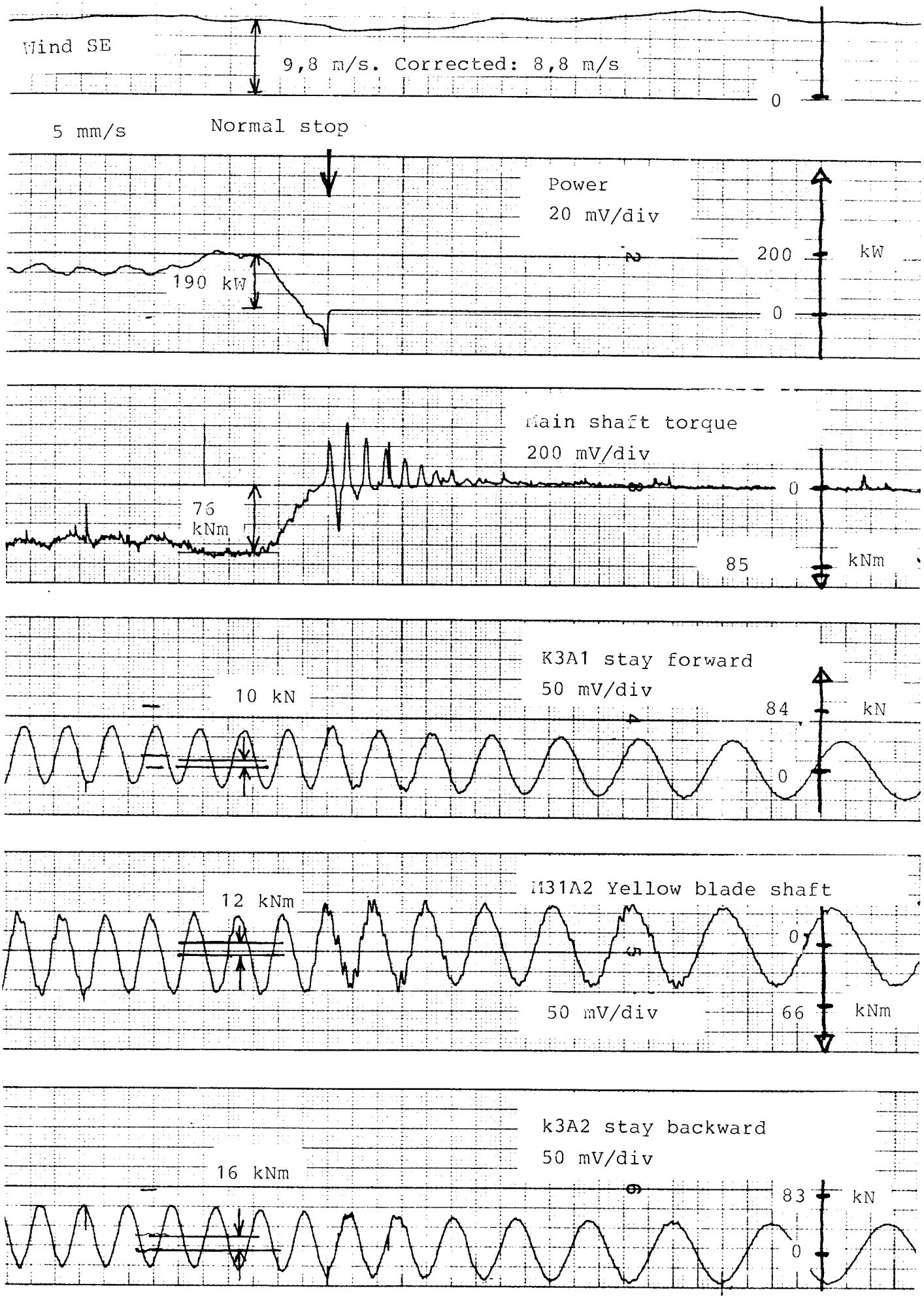
Wind SE
9,8 m/s. Corrected: 8,8 m/s
0
5 mm/s
Normal stop
Power
20 mV/div
200
kW
190 kW
0
Main shaft torque
200 mV/div
0
76
kNm
85
kNm
K3A1 stay forward
50 mV/div
10 kN
84
kN
0
M31A2 Yellow blade shaft
12 kNm
0
50 mV/div
66
kNm
k3A2 stay backward
50 mV/div
16 kNm
83
kN
0

Figure 3.16

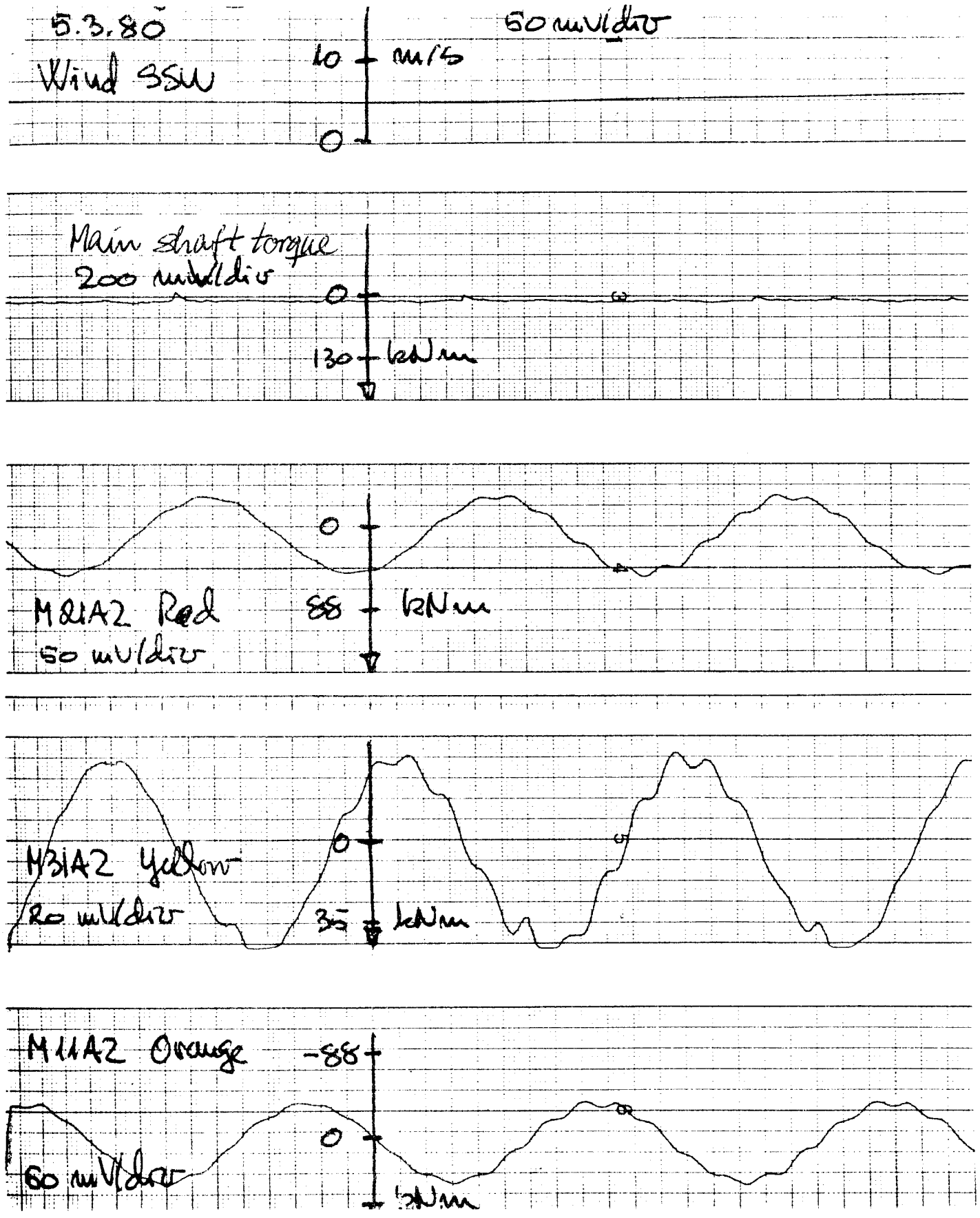
5.3.80
Wind SSW
10
m/s
0
50 mV/div
Main shaft torque
200 mV/div
0
130
kNm
0
M21A2 Red
50 mV/div
88
kNm
0
M31A2 Yellow
20 mV/div
35
kNm
M11A2 Orange
-88
0
60 mV/div
kNm

Figure 3.17

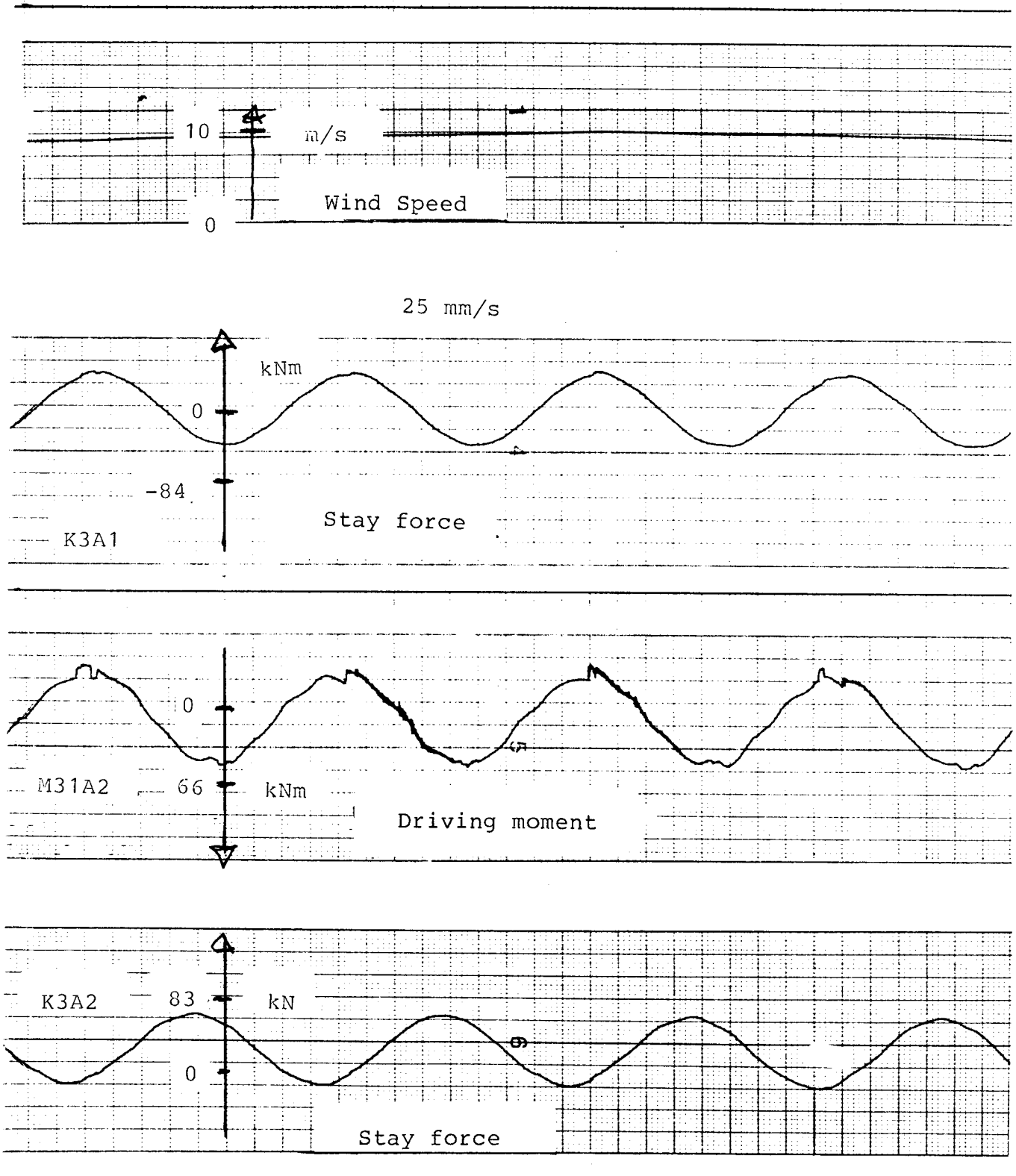
10
m/s
Wind Speed
0
25 mm/s
kNm
0
-84
K3A1
Stay force
0
M31A2
66
kNm
Driving moment
K3A2
83
kN
0
Stay force

Figure 3.18

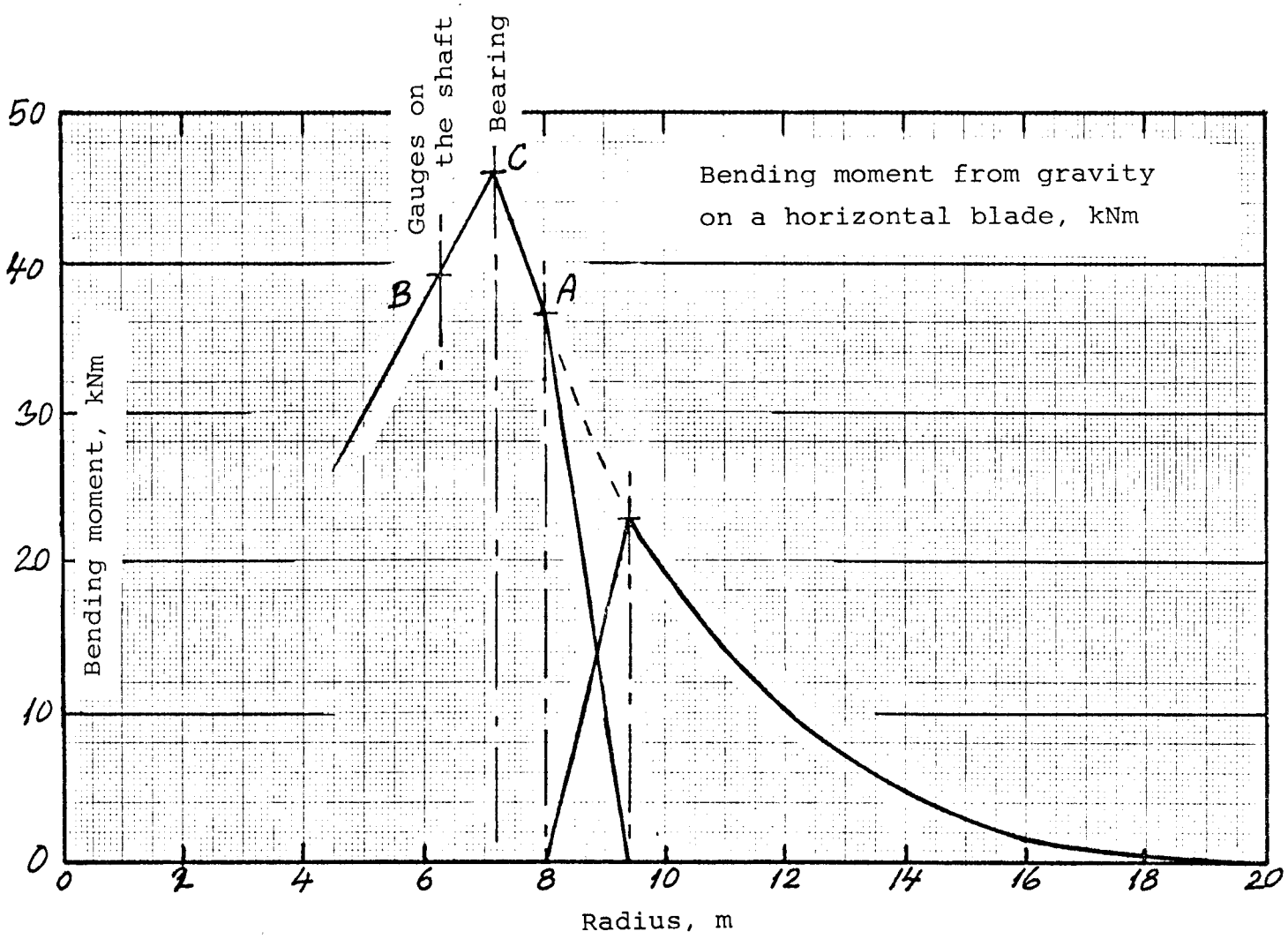

Figure 3.19

It should be noted that in both stays of Fig. 3.16 there are positive tensile forces. This means that the bearing seems to be sticking in the house and therefore carries a radial load which was unintentional. This could be the reason for the abnormal trace of the driving moment in Fig. 3.18.

3.7. Stresses due to gravity forces

The bending moment in the trunnion due to gravity is 37 kNm according to Fig. 3.19. The stress is correspondingly $\pm$ 24 MN/m^2. The superposed stress from the driving moment is of the order of 14 MN/m^2 at maximum power.

3.8. Deflections of the blade

Figure 3.20 shows a calculation of the blade deflection carried out by the Department of Engineering, Ole Gunneskov, Risø, ref. 3.2. The load case is calculated for a duty condition for which the power at the rotor shaft is 609 kW, the maximum power calculated at blade tip angle -4^{o}. The deflected shapes are shown for a pure radial blade in curve 1 and for a blade with cone angle 6^{o} in curve 2. The coning effect reduces the tip deflection by 25 % and the maximum axial bending moment in the steel shaft is correspondingly reduced by 40 % as shown in fig. 3.21.

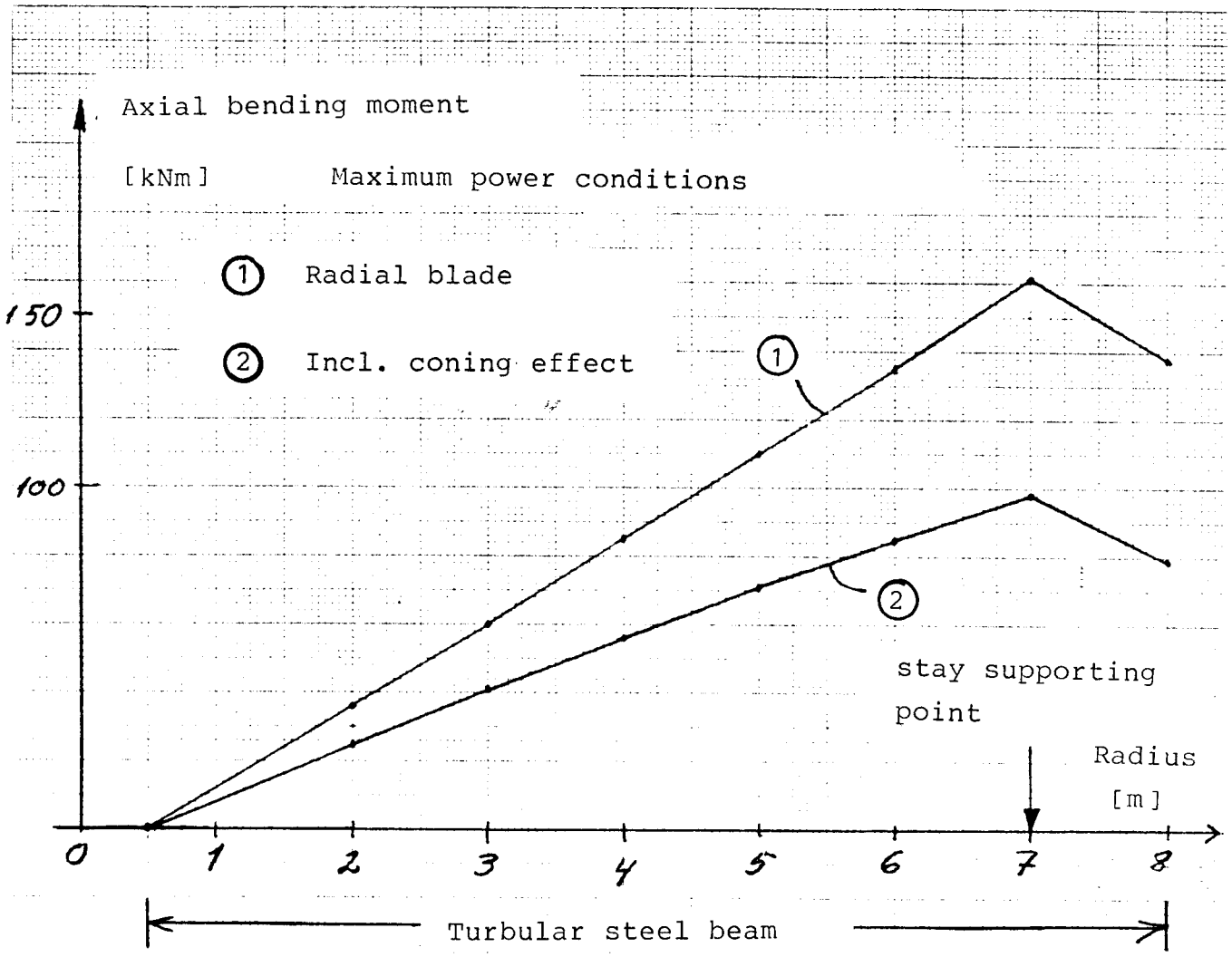

Figure 3.21

NIBE WINDMILL A - Deflections

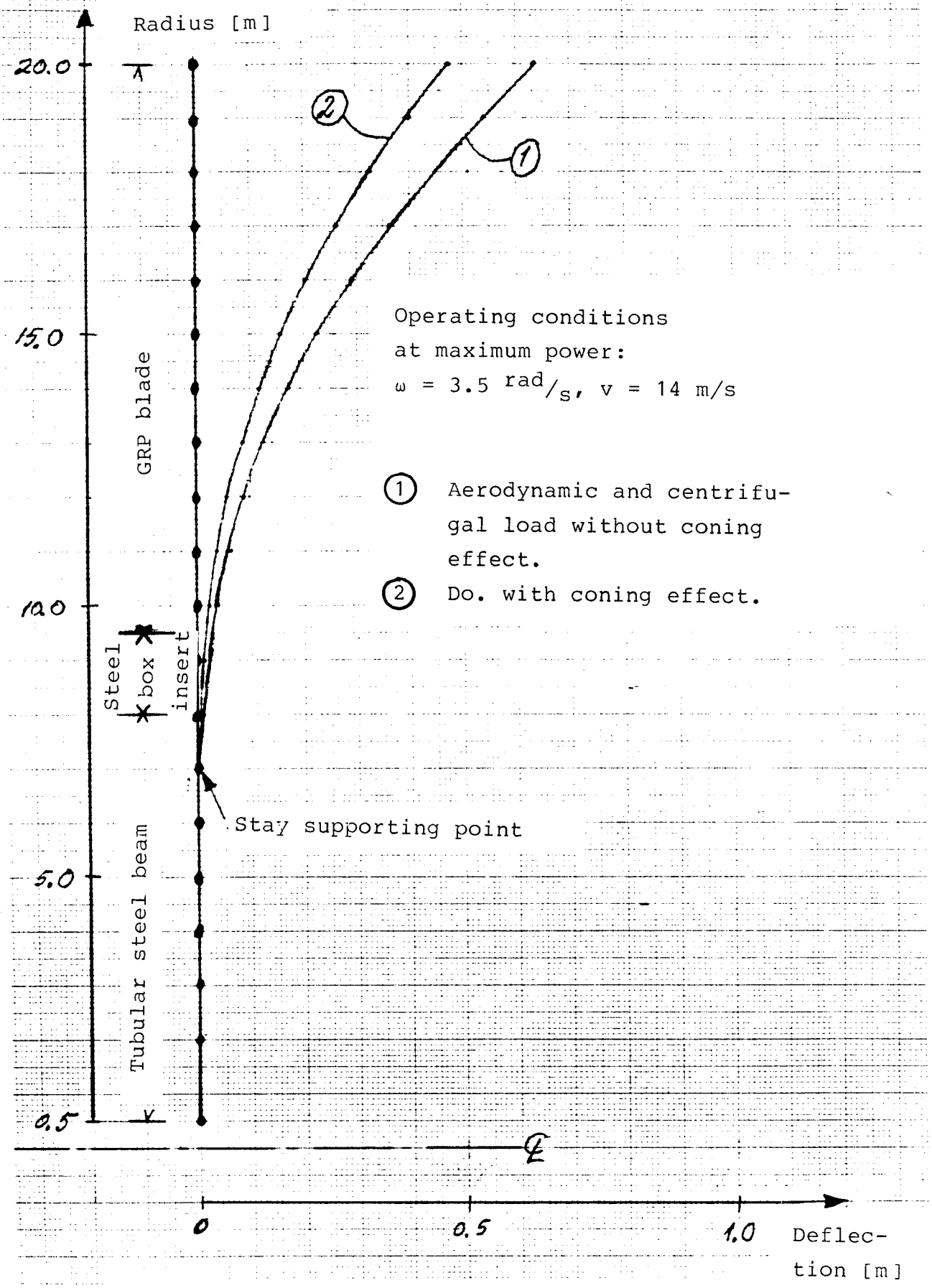

Figure 3.20

4. DISCUSSION

4.1. The preliminary measurement system.

This ad hoc measurement system was relatively easily established; the main problem was the influence of the measurement system on some of the channels shared with the turbine's microcomputer. After separating the system from the computer by amplifiers there have been no problems in the recording of operational parameters. The recording of the rotor channels has been hampered by noise caused by the long cables absorbing radio signals. This occasionally caused the strain gauge preamplifiers to oscillate, but modifications on the preamplifier installation have removed these oscillations.

The system has served - and still serves - as a means of obtaining preliminary data in a versatile way. This means that it may be used by interested persons with a minimum of instructions, thus permitting early assessments of turbine behavior and of the validity of the design calculations. Therefore a similar system will be established on the mod B turbine. The penalty is an accuracy of not better than 5-15%. The Brush plotter is not ideally suited because it is able to resolve frequencies far beyond the frequency range of interest in the wind turbines, while the amplitudes of the records are limited to about 5 cm. However, the plotter has proved reasonably reliable while standing unattended for several months in an unheated room in the turbine tower, and its ability to record up to 6 channels simultaneously has proved valuable.

4.2. The results

The measurement results are in good agreement with the predicted values. However, they also show some anomalies that should be investigated further.

The most pronounced characteristics of the stayed, stall-regulated mod A wind turbine as they appear from the measurements are:

- Gravity forces are clearly the most dominant in-plane forces. As indicated in Fig. 3.19 the in-plane struts play a very important role in keeping the resulting blade moment low.

- For the out-of-plane loads it is characteristic for a turbine which is regulated as the mod A turbine that during a normal stop sequence the blade passes through high lift coefficients to a stalled condition. This means that the blade is exposed to loads of the same magnitude as those at high wind speeds.

References

1.1: V. Askegaard, C. Dyrbye, S. Gravesen:
"Laboratory Tests on Gedser Wind Turbine's Blades".
Structural Research Laboratory, Technical University of Denmark. Report S 28/77 Nov. 1977.

1.2: P. Nielsen:
"Measuring Program for Two Windmills at Nibe, Denmark".
Proc. IEA Expert Meeting on LS-WEC's.
September 26-27, 1979, Boone, North Carolina, USA.

1.3: P. Lundsager, C.J. Christensen, S. Frandsen:
"The Measurements on the Gedser Wind Turbine 1977-1979".
The Wind Power Program of the Ministry of Commerce and the Electric Utilities of Denmark, November 1979.

1.4: P. Lundsager, C.J. Christensen, S. Frandsen, S.A. Jensen:
"Analysis of Data from the Gedser Wind Turbine Measurements 1977-1979".
The Wind Power Program of the Ministry of Commerce and the Electric Utilities in Denmark, May 1980.

2.1: B. Maribo Pedersen:
"Målinger på Nibemølle A, den 27. og 28. februar 1980" (Measurements on Nibe Wind Turbine mod. A, February 27th and 28th, 1980. In Danish). AFM Notat VK-62-800325.
Department of Fluid Mechanics, the Technical University of Denmark.

3.1: P. Lundsager, O. Gunneskov:
"Static deflection and eigenfrequency analysis of the Nibe wind turbine rotors. Theoretical Background".
Risø-M-2199, Nov. 1979.

3.2: O. Gunneskov, P. Lundsager:
"Static Deflection and Eigenfrequency Analysis of the Nibe Wind Turbine Rotors. Analysis and Results.
Risø-M-2200,(to appear).

Appendix A.

A Note about Wind Turbine Rotor Lay-Out Minimizing the Material Fatigue Problem

by Helge Petersen

An obvious feature of a blade which produces design problems is the division of the blade in order to pitch it. The two Nibe wind turbines shown in Fig. A1., are conventional in this respect.

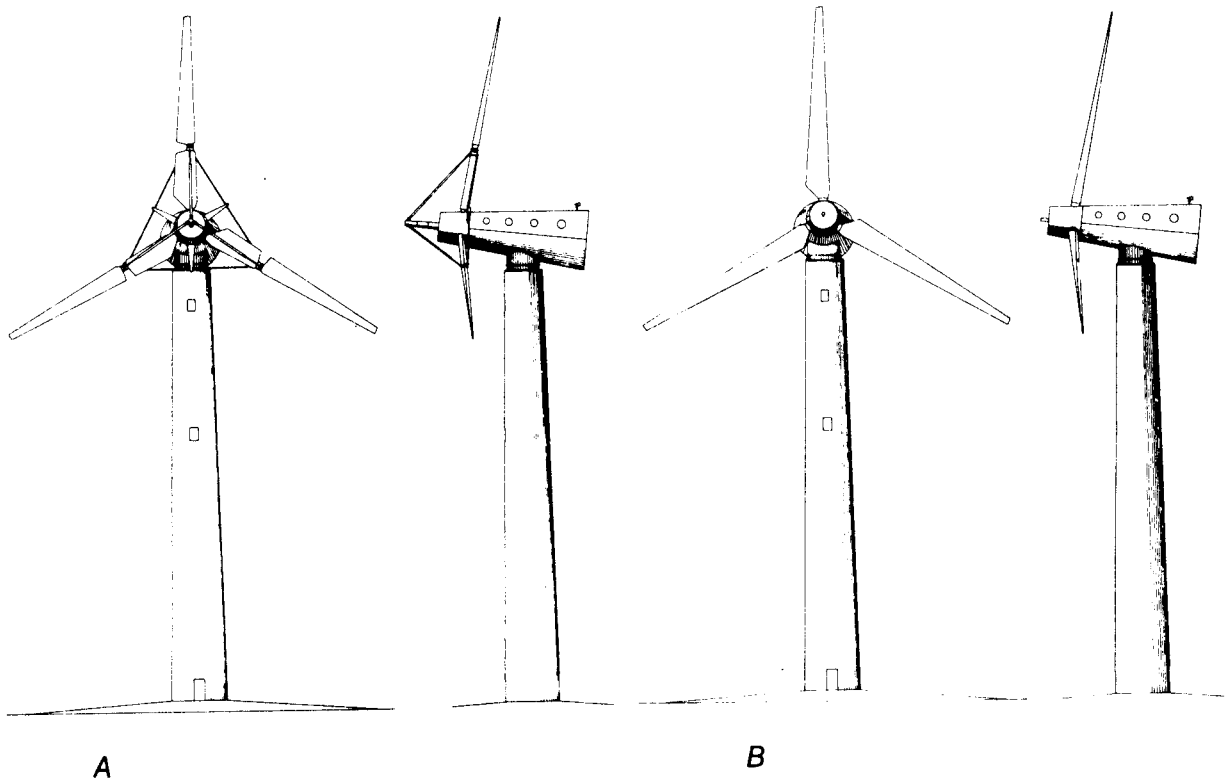

Figure A.1.

For the mod A the blade is divided in an outer and an inner blade part, the outer blade part is structually "shrunk" to be able to pass through the bearing at the end of the fixed inner blade part.

For mod B the whole blade is carried by a large bearing at the blade root and this limits the structural diameter.

Two other solutions are shown in Fig. A.2 and A.3, named Concept "29" and Concept "50", respectivily.

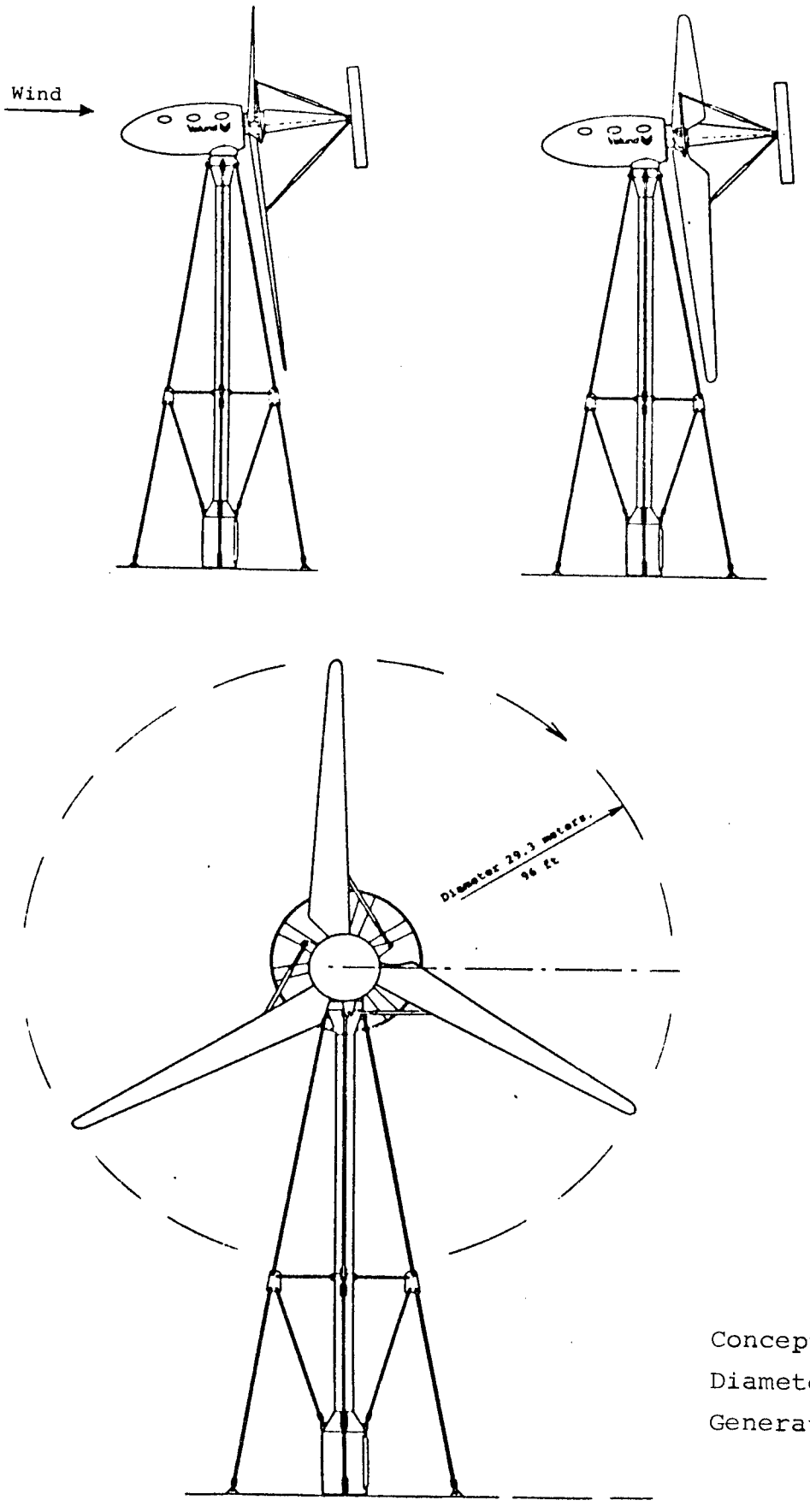

Concept "29"
Diameter 29 m
Generator 250 kW

Figure A.2

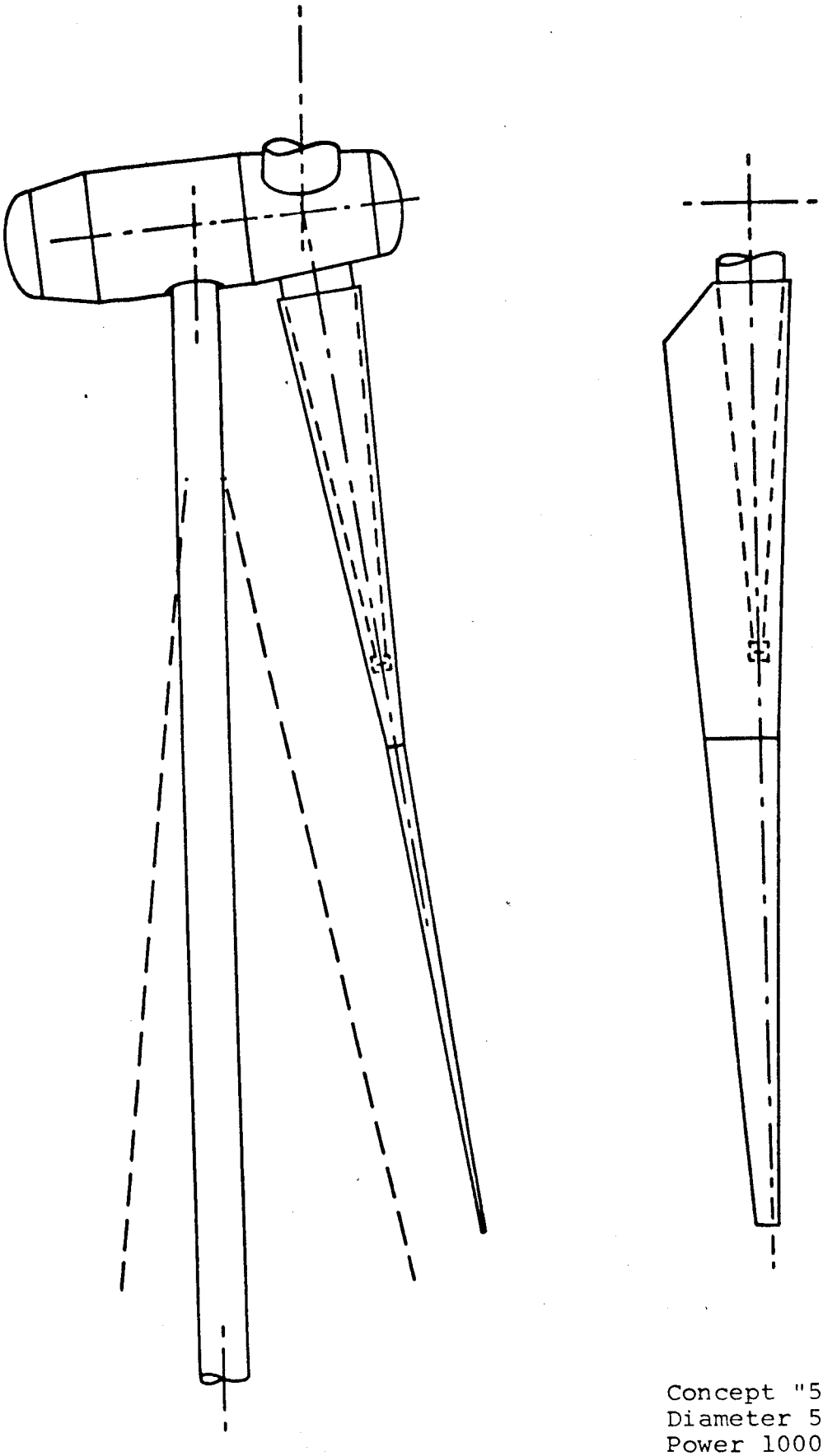

Concept "50"
Diameter 50 m
Power 1000 kW

Figure A.3.

The wind turbine in Fig. A.2, Concept "28", has strutted blades. However, the struts are hinged to the blade, the hinge being placed outside of the blade structure, and the root of the blade is hinged to the hub. Still the blade can pitch 90^{o}. In this way the blade structure is not interrupted by a shaft and bearing.

The wind turbine shown in Fig. A.3, Concept "50", has a cantilever structure fixed to the hub and surrounded by the hollow blade. This allows the blade to pitch around the carrying member. As for Concept "28" the bending moment decreases from the position of the outer bearing at the end of the carrying member towards the hub. In the carrying member of "50" the bending moment is zero at the outer bearing and increases towards the hub. However, it is less difficult to design a fixed structure strong enough to withstand the fatigue loads.

PART II: FLAPWISE BLADE VIBRATIONS IN THE NIBE A WIND TURBINE AT HIGH WIND SPEEDS. MEASUREMENTS, A POSSIBLE EXPLANATION OF THE PHENOMENON AND THE SUGGESTION OF A MODIFICATION OF THE STAY SYSTEM

1. Introduction

A preliminary measuring system has been established in order to obtain checks on the design assumptions and to monitor the behaviour of the stall-regulated Nibe Wind Turbine "A" during commissioning. A series of measurements has been reported in Ref. 1, and a separate series of measurements, during which the blade pitch angle was varied at wind speeds close to maximum power, has been reported in Ref. 2.

During the 24th to 25th of April 1980 a 24-hour test run with the turbine was started. At wind speeds in the range 12-16 m/s, using the preliminary measuring system, periods of strong flapwise blade oscillations were observed at a frequency corresponding to the 2 Hz of the first to the third fundamental flapwise eigenfrequency (Refs. 3 and 4).

Strip charts from the test run are shown in this note with a possible explanation of the mechanism that drives the phenomenon. If this explanation should prove to be correct, we would conclude that stall-regulated wind turbines ought to have relatively rigid blades. A modification of the Nibe "A" stay system is shown as a possible remedy should the phenomenon prove to be serious.

2. Measurements made 24-25 April 1980

Strip charts were taken of the channels listed below, using the measuring system as described in Ref. 1. The sensors coupled to the Brush writer were

1. Windspeed at 58 m height
2. Active power (kW)
3. Out of use
4. Trunnion moment orange blade
5. " " yellow "
6. " " red "

Fig. 2.1 shows the position of section 2, where the strain gauges are placed. From here the signal is transferred via preamplifiers with amplification 1000x and slip rings down to a Brush plotter at the bottom of the turbine tower (cf. Fig. 2.2).

On this occasion the Brush plotter was supplemented with a Hewlett-Packard frequency analyzer (Model 3721A) and an XY-plotter for the printout of frequency spectra.

Fig. 2.3 shows a record of a typical trace of a trunnion moment as was recorded earlier at relatively high wind speeds. The signal is mainly sinusoidal (gravity forces and wind shear) superposed by a two hertz oscillation (the fundamental flapwise frequency). The dynamic amplitude is approx. 20% of the static average of the signal.

Fig. 2.4 indicates an upstart recorded on 24 April 1980. For each revolution the trace has one very pronounced peak that is present also at very slow rotation; therefore, this can scarcely be called a dynamic effect in the blade. No explanation of this phenomenon has been found, but a possible one is that the channel is sensitive to radio waves; they will cause an offset of the signal level, although an offset as large as this has not been recorded earlier. The phenomenon seems to differ from that dealt with later.

Fig. 2.5 reproduces the frequency spectrum corresponding to the trace of Fig. 2.4 (above) compared with that corresponding to a normal trunnion moment signal (below). The spectra are shown with a linear frequency axis. The spectra should be taken with some reservation because the frequency analyzer could not be precisely adjusted to the signal; the frequency of the rotor is entirely dominant in the spectrum shown above, however, while a normal trunnion moment spectrum shows a further peak at the flapwise eigenfrequency.

Fig. 2.6 is a record of a sequence of the 24-hour run, at a time when the wind speed is approx. 12 m/s. There are short periods where oscillations at 2 Hz are dominant, and the corresponding spectrum is much like that shown in Fig. 2.5 below.

Fig. 2.7 illustrates a sequence of the 24-hour run where the wind speed is close to 15 m/s corresponding to a power production of more than 500 kW, i.e. the blades are close to a fully stalled condition. During a period of several minutes the dominant term in the signal is a 2-Hz flapwise oscillation, having a large

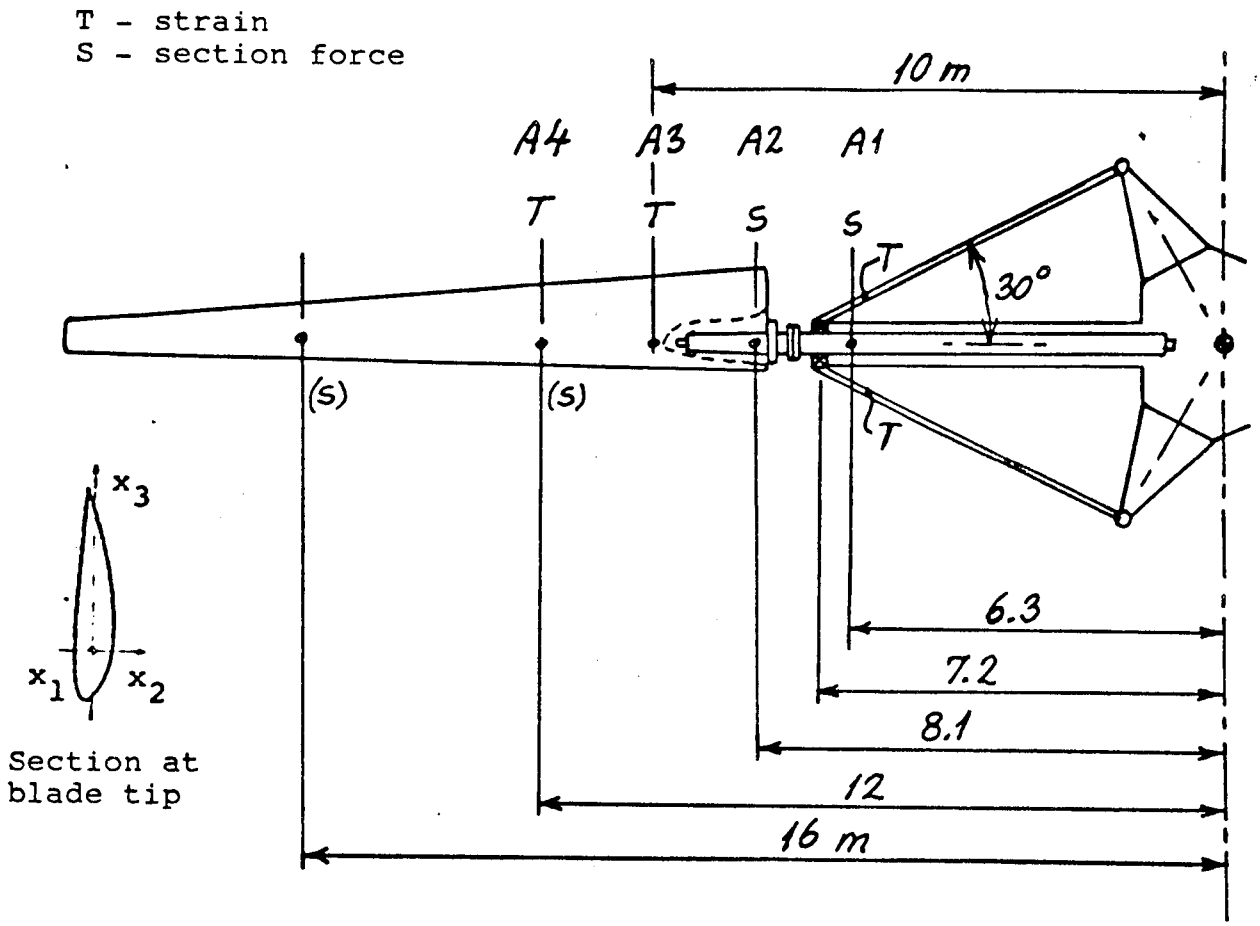

Figure 2.1

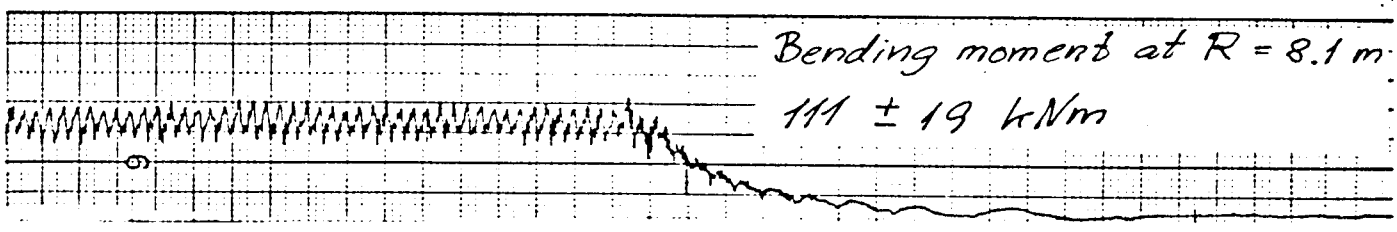

Figure 2.3

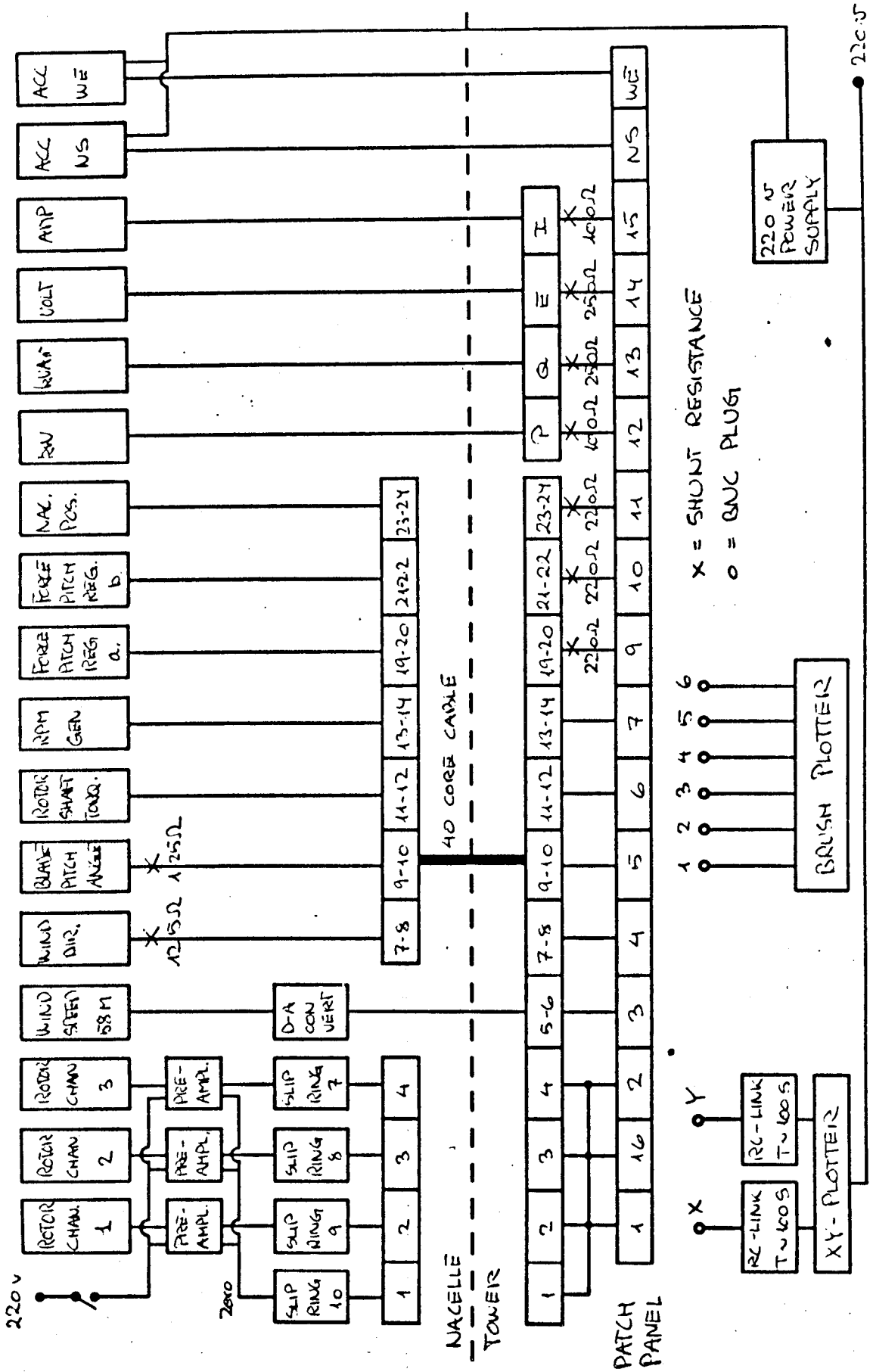
ROTOR
MAST
NACELLE
TOWER
ACC WE
ACC NS
AMP
VOLT
KWH
RPM
P
Q
E
I
12
13
14
15
WE
NS
220 V POWER SUPPLY
220 V
X = SHUNT RESISTANCE
O = BNC PLUG
BRUSH PLOTTER
RC-LINK TV 605
RC-LINK TV 605
XY-PLOTTER
X
Y
ROTOR CHAN. 1
ROTOR CHAN. 2
ROTOR CHAN. 3
PRE-AMPL.
PRE-AMPL.
PRE-AMPL.
SLIP RING 10
SLIP RING 9
SLIP RING 8
SLIP RING 7
200
WIND SPEED BSRN
D-A CONVERT
WIND DIR.
BLADE PITCH ANGLE
ROTOR SHAFT TORQ.
RPM GEN
FORCE PITCH REG. a.
FORCE PITCH REG. b
NAC. POS.
RW
40 CORE CABLE
NACELLE
TOWER
PATCH PANEL
125Ω
1 2 3 4 5 6
7-8
9-10
11-12
13-14
19-20
21-22
23-24
22Ω
40Ω
250Ω
400Ω

Figure 2.2

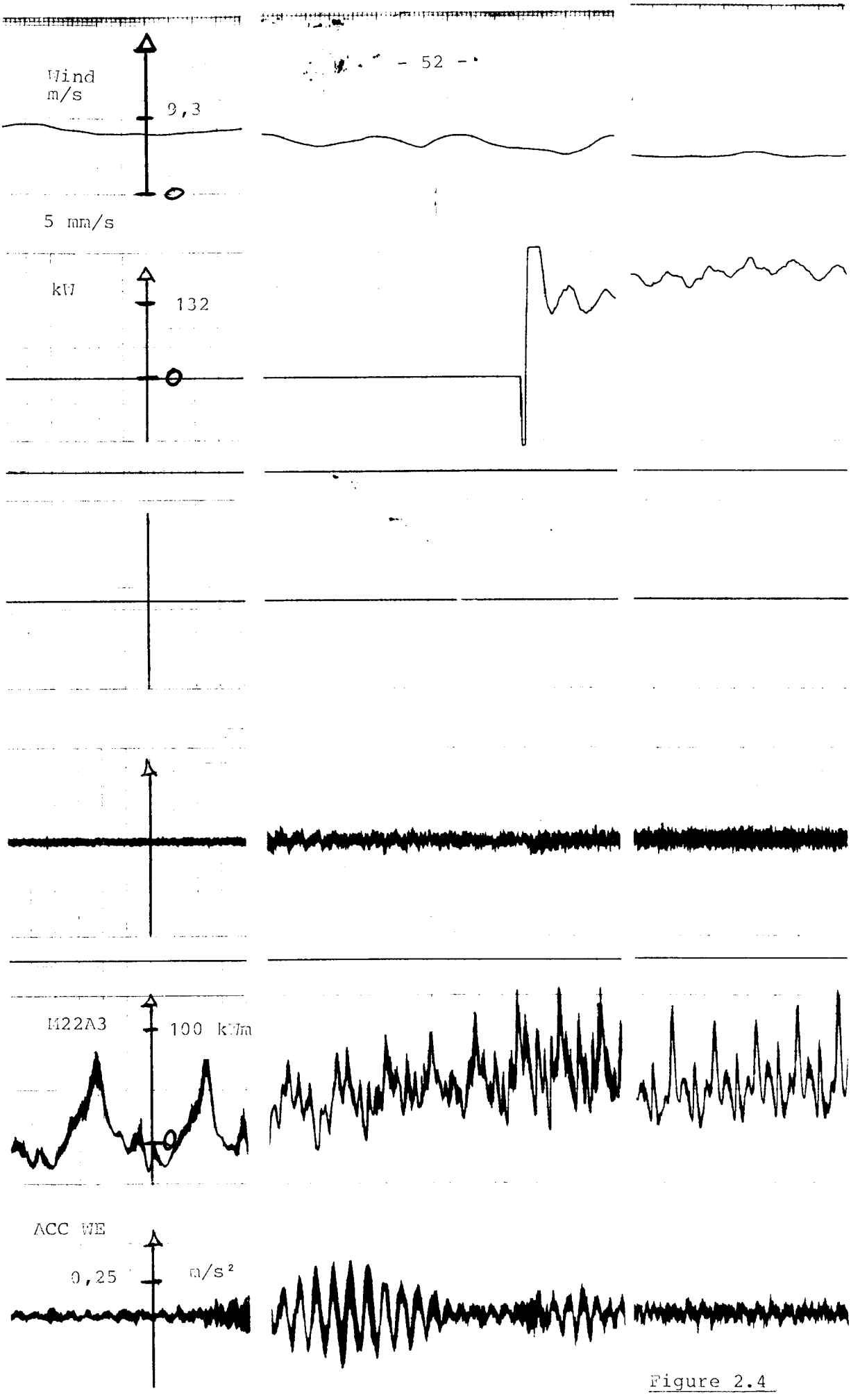

Figure 2.4

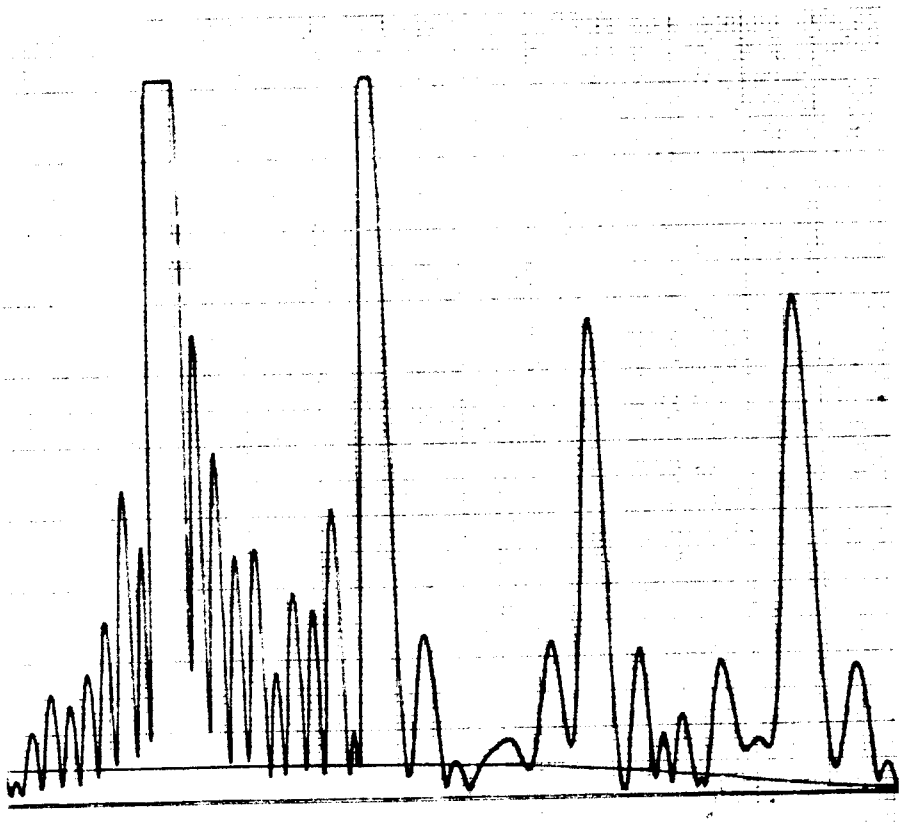

0 Frekvens Hz 2.5

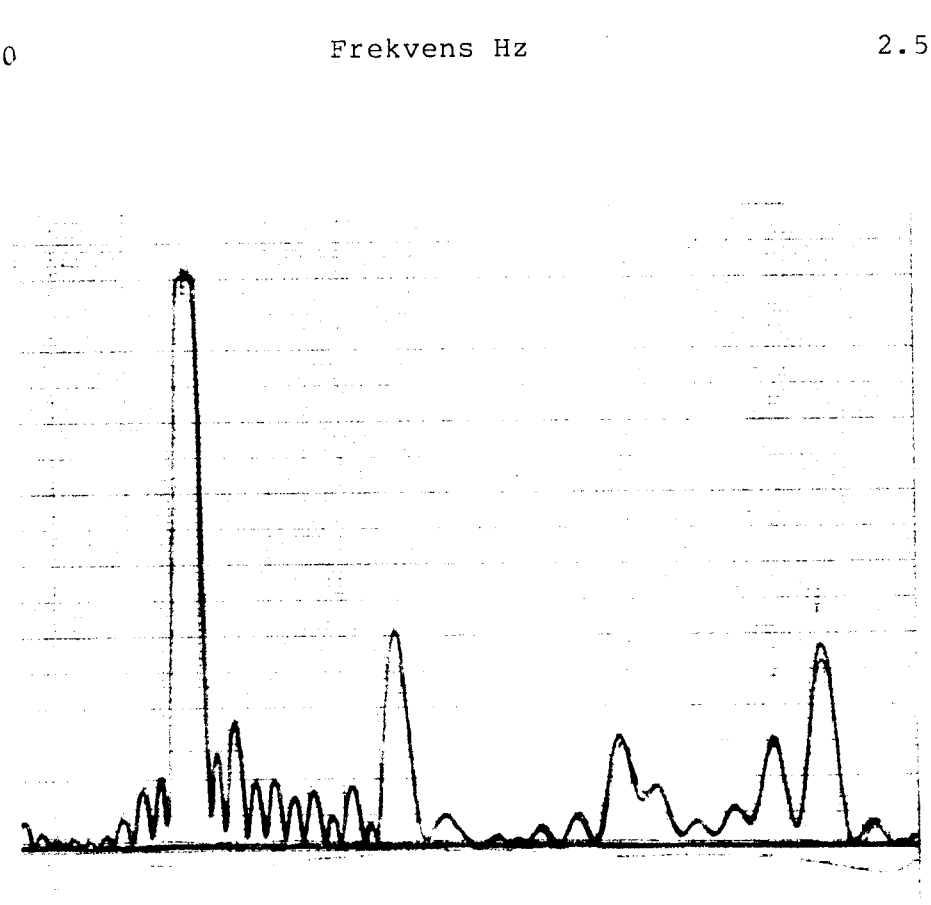

0 Frekvens Hz 2.5

Figure 2.5

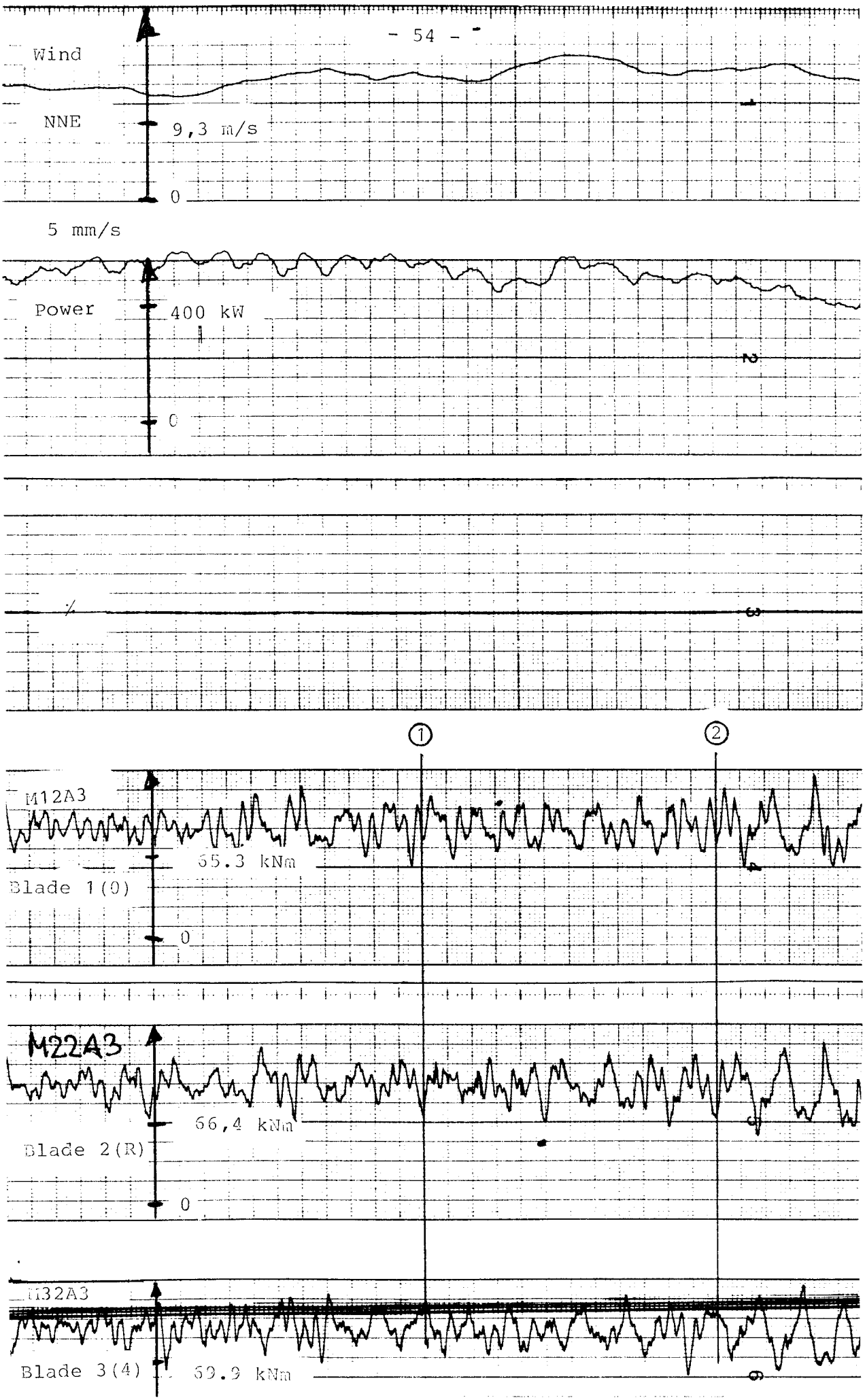
Wind
NNE
9,3 m/s
0
5 mm/s
Power
400 kW
0
%
①
②
M12A3
55.3 kNm
Blade 1(0)
0
M22A3
66,4 kNm
Blade 2(R)
0
M32A3
Blade 3(4)
59.9 kNm

Figure 2.5

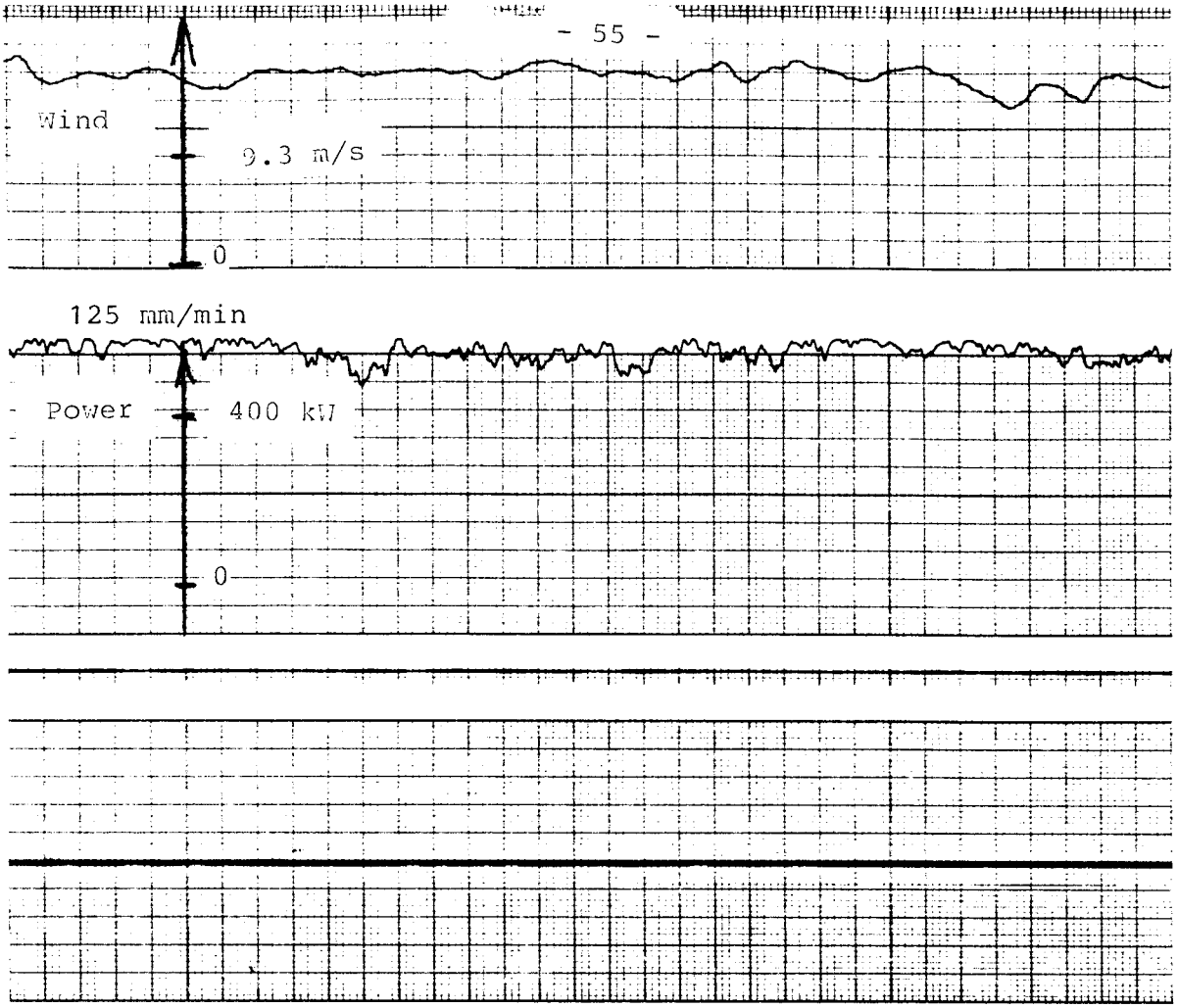
Wind
9.3 m/s
0
125 mm/min
Power
400 kW
0

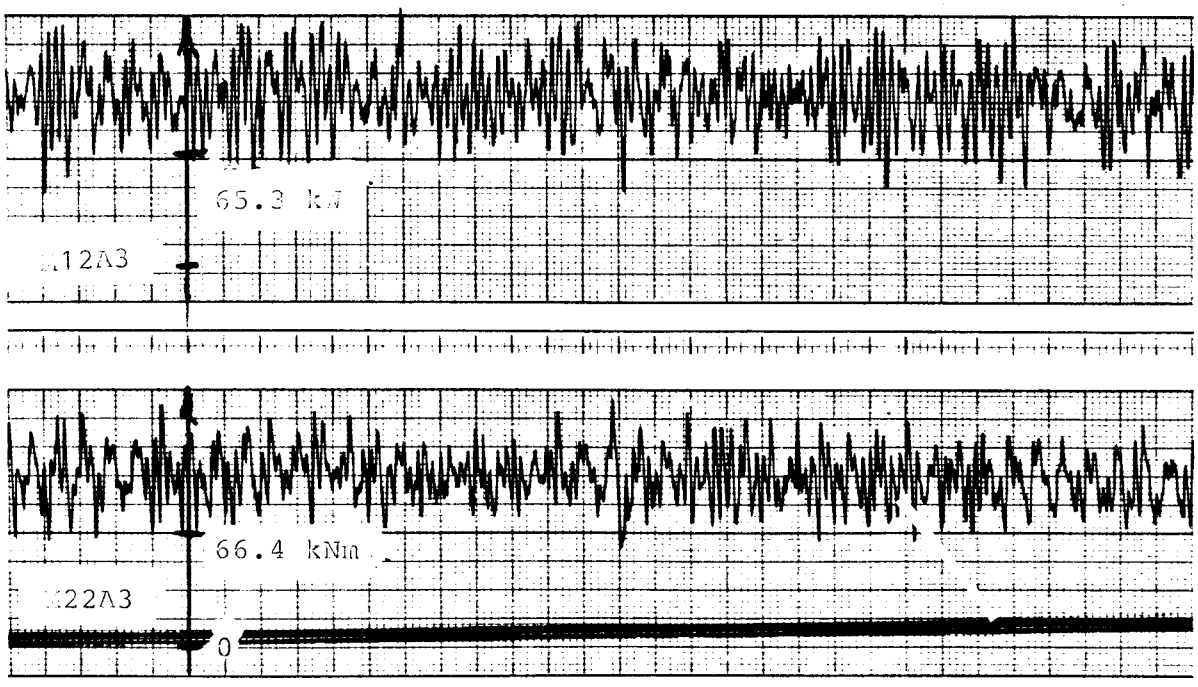
65.3 kW
M12A3
66.4 kNm
M22A3
0

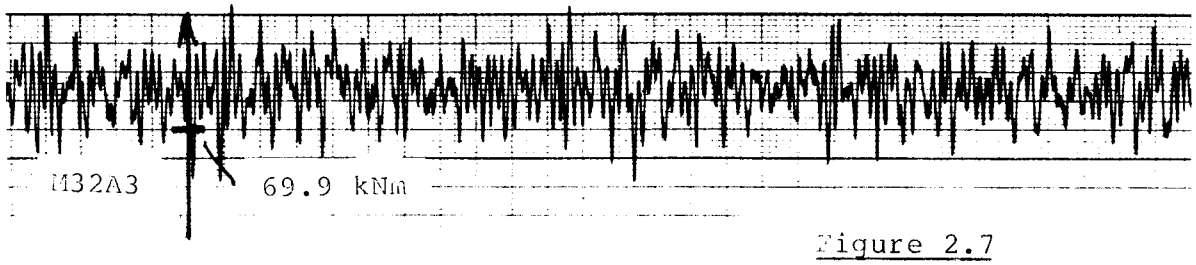
M32A3
69.9 kNm

Figure 2.7

amplitude. Although Figs. 2.6 and 2.7 are taken at different paper speeds the character of the signals in the two figures are clearly different from each other.

The spectrum corresponding to Fig. 2.7 is shown below in Fig. 2.8; a normal spectrum is shown in the above part of the figure. In the spectrum below the rotational frequency of the rotor is just visible; the flapwise fundamental frequencies, however, are dominant.

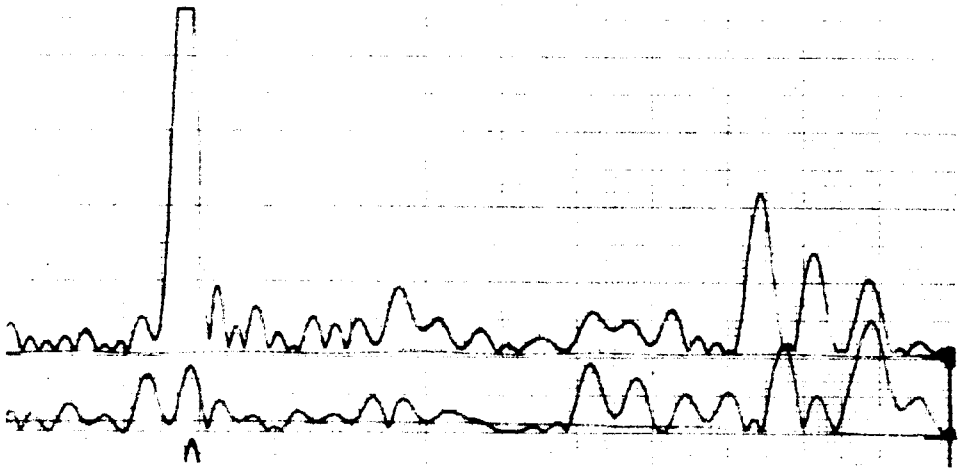

Fig. 2.8.

Table 2.1 shows a survey of the signals of Fig. 2.3 to 2.7. The phenomenon shown in Fig. 2.7 is clearly associated with dynamic amplitudes that are significantly larger than the amplitudes during normal operation. However,

Signal fig.	kW	Moment midd±ampl.	f ampl/stat
2.3	-	111±19 kNm	0.17
2.4	170	67±50 kNm	0.74
2.6	490	92±33 kNm	0.36
2.7	570	91±40 kNm	0.44

Table 2.1. Survey of trunnion moments.

the static averages are correspondingly lower, so that the maximum moments are the same as during normal operation.

This phenomenon is observed at windspeeds similar to those present during the measurement series reported in Ref. 2, where the phenomenon was not observed. However, at that location the wind speeds were slightly lower than on 25 April, and the degree of turbulence was markedly lower.

In the following sections stall-induced vibrations are investigated as a possible explanation of the oscillations.

3. Single degree of freedom model for stall-induced oscillations

One possible explanation of the oscillations is that they are caused by so-called stall flutter, i.e. stall-induced vibrations. In order to investigate this possibility, a simple one degree of freedom model has been established, so that the principal features of the phenomenon may be investigated and compared with the measured response of the turbine.

In this chapter the equations are derived that describe stall-induced oscillations of a blade tip of a stall-regulated wind turbine. The most important simplifying assumptions are:

a. The air flow is laminar, homogeneous, and has the constant velocity v_n parallel to the rotor axis.

b. The tip movement is supposed to have one degree of freedom, perpendicular to the rotor plane. The reason for this is that the mechanism is supposed to rest on the lowest flapwise eigenmode for a single blade.

c. The wind load on the blade is supposed to have a piecewise linear dependency on the angle of incidence. In this way the load term of the equation of motion is linearized.

d. The angle of incidence is computed directly from the wind speed v_n. The reason for this is that at the power level where the phenomenon is assumed to be significant, the aerodynamic efficiency is small and the axial induction factor therefore is correspondingly small.

e. The development is based on the deflection of the blade tip. The reason for this is that the load as well as the displacement is largest at the tip; therefore the tip deflections determine whether or not the phenomenon occurs.

We consider a configuration as shown in Fig. 3.1.

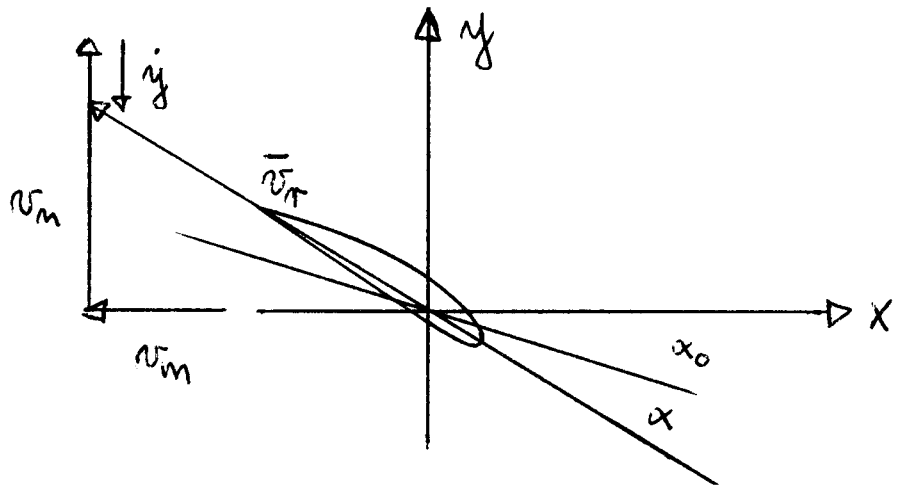

Fig. 3.1. Configuration of blade tip.

The figure shows the blade tip that moves in the positive x-direction with the translational velocity v_m due to the rotation of the rotor. The tip is influenced by the wind speed v_n, acting in the positive y-direction. The tip has the pitch angle α_o relative to the rotor plane, and the relative wind velocity vector $\bar{v}_v$ has the angle of attack α to the tip chord. It is assumed that blade deflections cause the tip to move in the y-direction only, and by including the velocity $\dot{y}$ of this movement (i.e. assuming that $\dot{y}$ is not small compared to v_n) the following relation is obtained:

$$\alpha = \left(\frac{v_n}{v_m} - \alpha_o\right) - \frac{\dot{y}}{v_m} \qquad (1)$$

The first term corresponds to the angle of attack $\bar{\alpha}$ during stationary conditions, while the second term is the change in α due to oscillations. Thus,

$$\alpha = \bar{\alpha} - \frac{\dot{y}}{v_m}$$

$$\bar{\alpha} = \frac{v_n}{v_m} = \alpha_o$$

The load acting on the blade tip is a function of α.

The tip movement is described by the equation

$$\ddot{y} + 2\zeta\omega\dot{y} + \omega^2 y = p(\alpha) \qquad (3)$$

i.e. the description is based on the fundamental frequency ω, the structural damping ratio ζ, and the load $p(\alpha)$, and that due to Eq. (2) depends on $\dot{y}$. Thus the linear equation (3) has a load term that couples to the solution because of the dependency on $\dot{y}$. This coupling is linearized by introducing the piecewise linear load shown in Fig. 3.2. This curve form is a

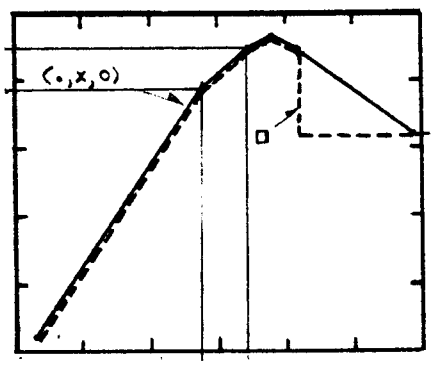

Fig. 3.2. Piecewise linear load.

realistic one for a tip profile, as can be seen by comparing it with the curves in Fig. 3.3. The load assumption then becomes

$$p_i(\alpha) = a_i\alpha + b_i \qquad \alpha_i \leq \alpha \leq \alpha_{i+1}, \qquad (4)$$

where

$$a_i = (p_{i+1} - p_i)/(\alpha_{i+1} - \alpha_i), \text{ and}$$

$$b_i = p_i - a_i \cdot \alpha_i \ .$$

By introducing the load Eq. (4) into Eq. (3) we find

$$\ddot{y} + (2\zeta\omega + \frac{a_i}{v_m})\dot{y} + \omega^2 y = a_i\bar{\alpha} + b_i \qquad \alpha_i \leq \alpha \leq \alpha_{i+1}, \tag{5}$$

where the limits α_i correspond to the velocities

$$\dot{y}_i = (\bar{\alpha} - \alpha_i) \cdot v_m . \tag{6}$$

Thus, Eq. (5) is valid in the velocity range

$$\dot{y}_i \leq \dot{y} \leq \dot{y}_{i+1} .$$

Assuming initial values y_i^o and $\dot{y}_i^o$ at the time t_o, in this interval Eq. (5) has the solution

$$y = y_s + C_i e^{-\beta_i t} \cos(\omega_i t - \phi), \tag{7}$$

where

$$\begin{aligned} y_s &= (a_i\bar{\alpha} + b_i)/\omega^2 \\ \omega_i &= \sqrt{\omega^2 - (0.5\ \beta_i)^2} \\ \beta_i &= \beta + a_i/v_m \\ \phi_i &= \omega_i t_o - \arctan[(\dot{y}_i^o/(y_i^o - y_s) - \beta_i)/\omega_i] \\ c_i &= (y_i^o - y_s) e^{\beta_i t_o}/\cos(\omega_i t_o - \phi_i) \end{aligned} \tag{8}$$

If a_i is negative and has a sufficiently large numerical value for β_i to be negative, the solution in this interval is not damped but increasing.

This means that if the blade enters a displacement pattern where the angle of attack α pendle across the maximum of the load curve Fig. 3.2, stationary oscillations may occur in which each period consists of a part with negative damping β_i, where energy is into the movement, and a part with positive damping, where energy is taken from the movement.

With a load as that shown in Fig. 3.2 the amplitudes of the movement cannot increase arbitrarily, because the damping on the part of the curve with positive slope will take energy from the movement. Therefore, the term stall flutter is not indicative of

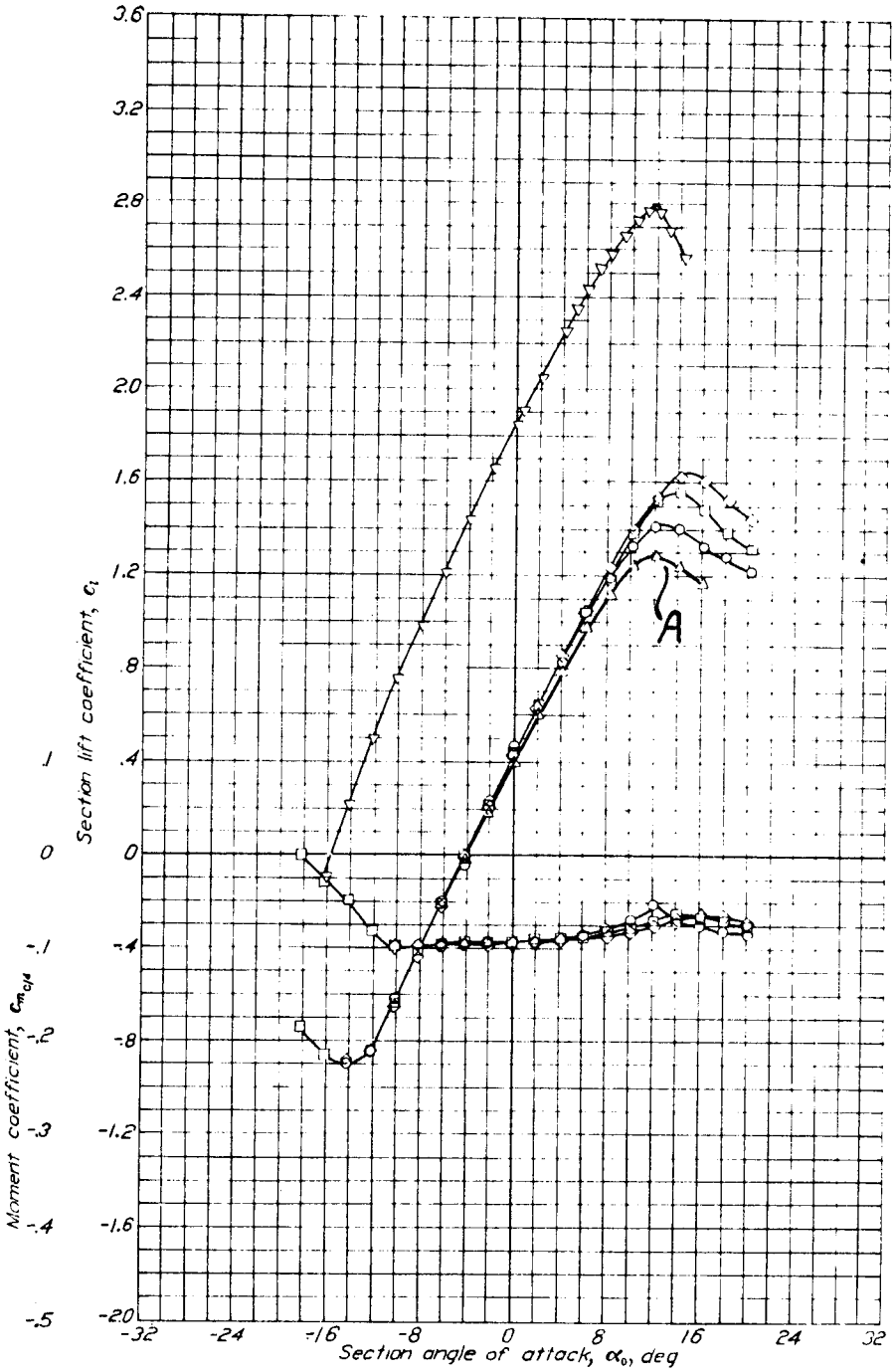

Fig. 3.3. Aerodynamic coefficients for the blade profile NACA 4415, that is, the tip profile for the Nibe turbines at radius 18 m, 2 m from the blade tip. The curve A shows the lift coefficient C_L versus the angle of attack α for this profile, when it has some specified roughness close to the leading edge.

the mechanism which consists of stationary oscillations of limited amplitude.

The equations shown above are coded in a FORTRAN IV program that solves the equation of motion by simulation. The blade tip is given an initial displacement and/or velocity, and then the movement is described stepwise over a number of revolutions sufficiently large to determine if the oscillation dies down or develops into a stationary oscillation.

In the program the load is applied in the following way: It is seen from Eq. (3) that the load corresponding to a static displacement y_s^i is

$$p_s^i = \omega^2 y_s^i. \qquad (a)$$

If the wind load distribution for the actual blade at a given wind speed v_i is calculated, this wind load distribution may be applied on a finite element model of the blade whereby the tip displacement y_s^i may be found. By means of Eq. (9) the load to be used in the dimensionless Eq. (3) may be determined. If this is repeated for a number of wind speeds the load curve Fig. 3.2 may be described at the degree of sophistication that is judged to be necessary.

4. Calculated results for a duty condition

In this chapter some results are shown that are computed using the model for a pitch angle $\alpha_o = -4$ deg corresponding to the setting at high wind speeds. The wind load is prescribed as described in Chapter 3 with a wind load distribution taken from Ref. 5, and with tip deflections computed by the beam model described in Ref. 3. The resulting wind load is shown in Fig. 4.1.

In Fig. 4.2 some results are shown from a series of calculations made for varying wind speed v_n. The influence of the ratio ζ of structural damping is shown. Due to the simplifications inherent in the model, absolute values of the results should be taken with some reservation. However, it seems reasonable to draw the general conclusions given below.

With a smooth load curve (i.e. a curve without pronounced corners), stationary stall-induced oscillations may occur spontaneously at a well-defined wind speed v_n^o. This wind speed most probably corresponds to that at which the stall reaches the blade tip, which is 13-15 m/s for the Nibe "A" turbine. When stationary oscillations occur the dynamic amplitude is of a large magnitude, and it rises with increasing wind speed. Oscillations may occur at wind speeds below v_n^o, which is the case for the load curve indicated with dotted lines in Fig. 4.1. However, this demands initial disturbancies of a magnitude that is considerable, especially for the smooth curve.

Most probably, therefore, under realistic conditions these oscillations may occur periodically in a range of wind speeds of a limited extent around v_n^o, preferably in turbulent wind. The oscillations may be initiated by a gust, and they may be stopped again by another gust. The patterns shown in Fig. 2.6 and 2.7, although mutually different, are expected to be typical for this phenomenon.

Changes in the structural damping within realistic limits have only a small influence on the results, while the shape of the load curve has a large influence. The wind speed v_n^o seems to be determined by the maximum of the curve, but the magnitude of the oscillations seems to depend on the sharpness of the maximum. If the curve has a jump as indicated in Fig. 4.1, the phenomenon may occur in a significantly larger wind speed range as indicated in Fig. 4.2. If the curve has a plateau at the maximum such large starting amplitudes are required that the phenomenon will scarcely take place.

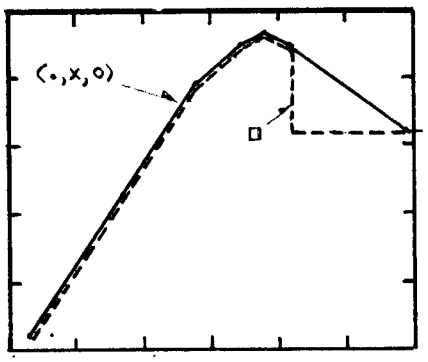

Fig. 4.1. Wind load applied in the model.

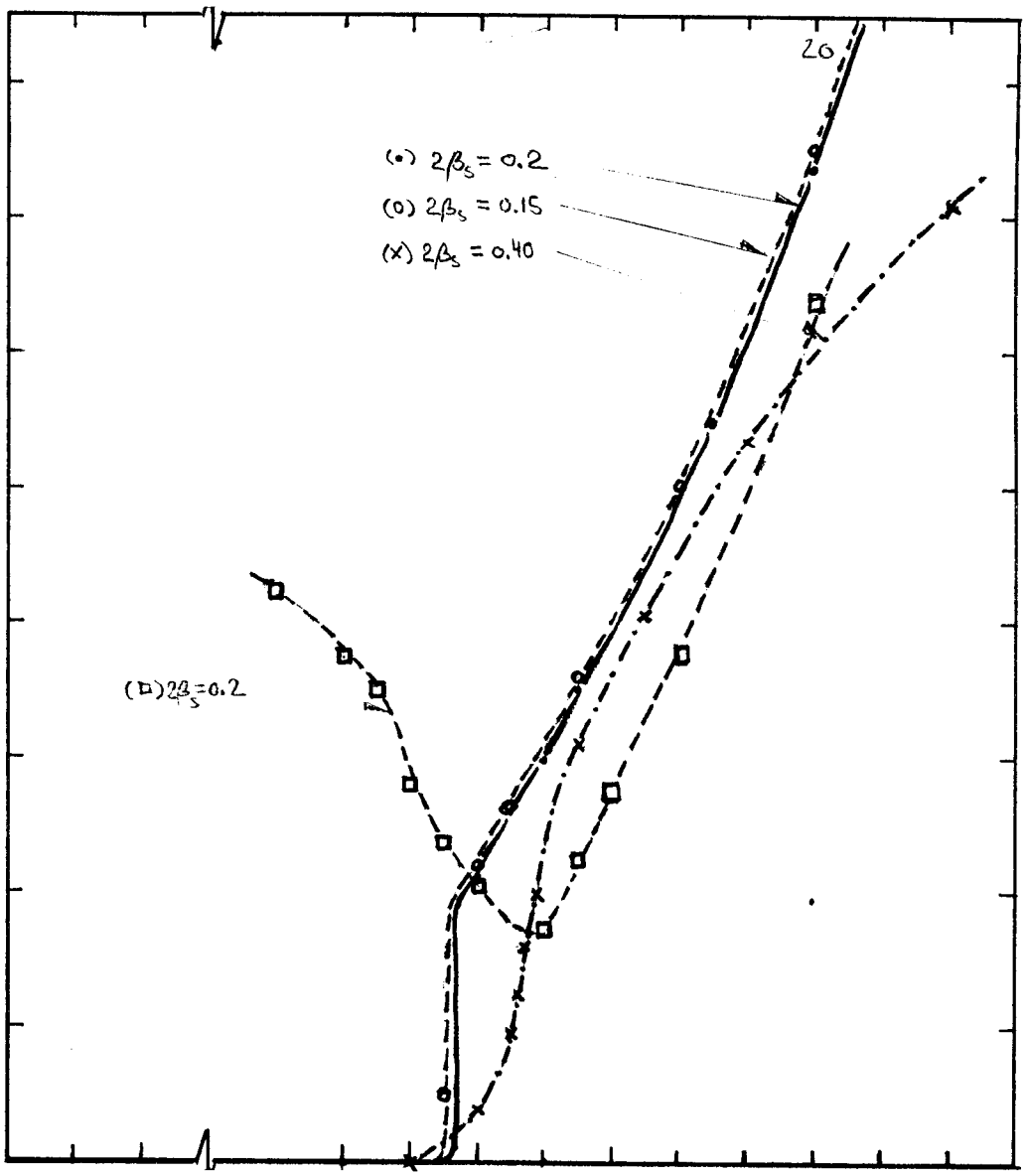

Fig. 4.2. Results for pitch angle α_o = -4 deg.

A gross estimate of the tip deflections that correspond to the measured moment amplitudes may be made as follows: The average moment at high wind speeds is approx. 100 kNm, which, according to Fig. 3.2 of Part I corresponds to a tip deflection of the order of magnitude 0.6 m. The moment amplitude of the magnitude 40 kNm therefore corresponds to displacement amplitudes of the order 0.25 m, while Fig. 4.2 predicts displacement amplitudes of 0.40 m.

The conclusions based on these calculations are

- stall-induced vibrations may occur if the axial wind load has a maximum at a certain wind speed;
- there is a maximum, the vibrations most probably will occur in a range of wind speeds around the maximum; the size of the range seem to increase with the sharpness of the maximum;
- since the mechanism is based on the influence of the displacement velocity on the angle of attack, stall-induced vibrations seem to be most probable for stall-regulated wind turbines having flexible blades.

5. Evaluation of measured results

Fig. 5.1 shows the magnitudes of the measured trunnion moments Fig. 2.3 and Fig. 2.7 and Table 2.1. The magnitudes are shown relative to those predicted computationally in the so-called load spectrum, dealt with in Ref. 4 and originally published in a note AFM VK-22-780108 "Belastninger på rotorblad, rotor A" ("Loads on rotor blade, rotor A"). Here the spectrum is converted to trunnion moments.

It appears that the trunnion moments of Fig. 2.3, the normal duty condition at a power output of approx. 500 kW, agree well with the load spectrum.

The trunnion moments of Fig. 2.7 have characteristics that are different from those found in the load spectrum. This is reasonable because they are not as such included in the load spectrum, and they should therefore be considered as loads to be added to the spectrum in the evaluation of the lifetime of the blades.

If it is assumed that the trunnion moments of Fig. 2.7 occur in approx. 2% of the time of operation the number of such moment cycles will be approx. 10^6 per year or $3 \cdot 10^7$ during 30 years. This is significant if the corresponding stresses are high; in this case the stresses should be evaluated.

The steel trunnion has the outer and inner diameters 282 mm and 210 mm, respectively, so that the cross-sectional moment of

inertia is $2.15 \cdot 10^{-4}$ m^4. From Table 2.1 the largest and the smallest trunnion moments, 131 kNm and 51 kNm, respectively, are taken, leading to the corresponding stresses 86 N/mm^2 and 33 N/mm^2. This stress range cannot be considered small for such a large number of cycles.

If these results are judged to reduce the expected lifetime drastically, and if it therefore is considered desirable to suppress the oscillations, it may be done by means of a modification of the stay system as shown in Fig. 5.2. A point on the blades near the tip at radius 18 m is connected to the hub by stays pointing forward. If this is done, it will seem natural at the same time to interconnect the blades by means of stays as shown in the figure. By doing this, the oscillating loads due to gravity forces may be significantly reduced.

6. Conclusion

During measurements on the Nibe "A" wind turbine 24 and 25 April 1980, using the preliminary measurement system, flapwise oscillations were observed at a frequency of 2 Hz and with significantly large amplitudes of the order ±50 kNm in the steel trunnion. The oscillations occurred periodically at wind speeds 13-16 m/s at power output 500 kW and above. Wind direction was NNE; the air was rather turbulent. Durations from a few seconds to more than one minute were observed.

One possible explanation is that the phenomenon is caused by stall-induced stationary oscillations, and results from computations using a simple one degree-of-freedom model of a blade tip are given. The results show that such oscillations are possible, and that if this should be the case then the following ought to be expected for the Nibe "A" wind turbine:

a. The oscillations should be expected to occur periodically, especially in turbulent wind at a power output above 500 kW.

b. The observed amplitudes of ±50 kNm do not represent any immediate danger for the rotors. However, the implications for the fatigue life should be considered.

c. An extension of the operational wind speed range above 15 m/s should be accompanied by measurements.

If these oscillations prove to be a problem, they may be suppressed by means of a modification of the stay system, whereby the blade tips are connected to each other and to the hub by means of additional stays.

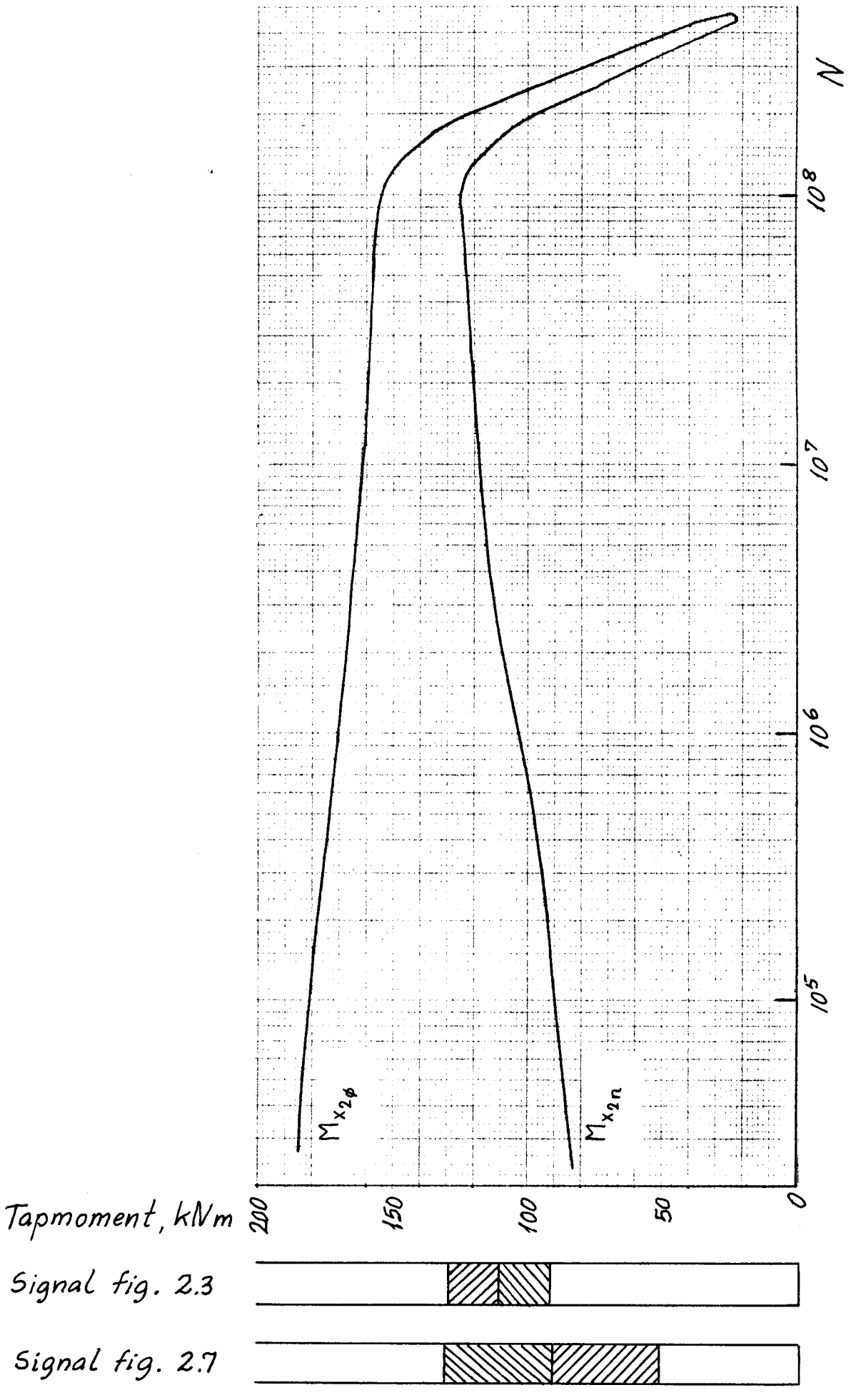
N
108
107
106
105
$M_{x2\phi}$
M_{x2n}
Tapmoment, kNm
200
150
100
50
0
Signal fig. 2.3
Signal fig. 2.7

Figure 5.1

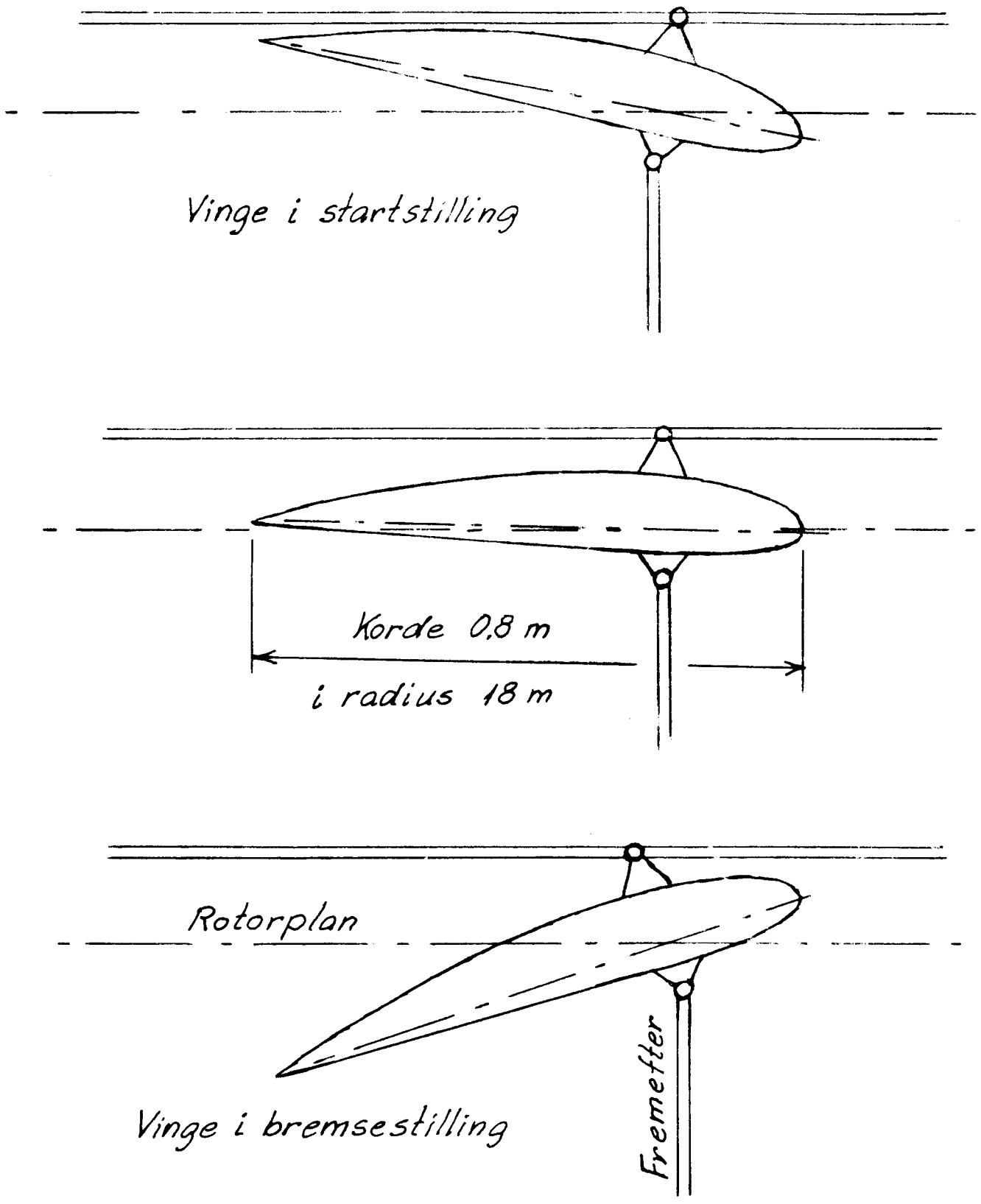
Vinge i startstilling
Korde 0,8 m
i radius 18 m
Rotorplan
Fremefter
Vinge i bremsestilling

Figure 5.2

References.

1. P.Lundsager, H.Petersen.
"Preliminary results from blade load measurements for the Nibe "A" wind turbine". Paper presented at 4th expert meeting "Rotor Blade Technology with special respect to fatigue design problems". Stockholm April 21nd and 22nd 1980.

2. B.Maribo Pedersen.
"Målinger på Nibe mølle A den 27. og 28. februar 1980". (Measurements on the Nibe A windmill, february 27. og 28. 1980. In Danish). AFM note VK-62-800325, Dept. of Fluid Mekanik, Techncal University of Denmark.

3. P.Lundsager, O.Gunneskov.
"Static deflection and eigenfrequency analysis of the Nibe wind turbine rotors. Theoretical background". Risø-M-2199, November 1979.

4. H.Petersen.
"Rotorkonstruktionen for de to Nibe Vindmøller opført af elværkerne". (The rotor design for the two Nibe windmills erected by the electric utilities. In Danish)

5. B.Maribo Petersen m.fl.
"Status for mølle A". (Status for windmill A. In Danish) AFM note VK-62-800325, Dept. of Fluid Mekanik, Technical University of Denmark.

Risø National Laboratory **Risø - M - 2253**

Risø - M - 2253

Title and author(s)

The dynamic behaviour of the stall-regulated A wind turbine. Measurements and a model for stall-induced vibrations.

P.Lundsager, H. Petersen, and S.Frandsen

Date
November 1981

Department or group
Department of physics

Group's own registration number(s)

70 pages + tables + illustrations

Abstract

The report is in two parts. In the first part the preliminary measurement system used is described, and a survey of the measurements made until the end of March 1980 is given. Results are presented concerned with the measurements of tower eigenfrequencies, eigenfrequencies of the stationary rotor and the characteristics of both flapwise bending moments. The findings are compared with the design assumptions, and the agreements is found to be good. In the second part the possible occurrence of stall-induced blade vibrations is investigated. Vibrations with first flapping eigenfrequency are reported and a one degree of freedom model with velocity-dependent load is presented. Calculated results are shown with agree reasonably well with measured characteristics. A possible modification of the stay system is suggested.

Copies to

Available on request from Risø Library, Risø National Laboratory (Risø Bibliotek), Forsøgsanlæg Risø), DK-4000 Roskilde, Denmark
Telephone: (03) 37 12 12, ext. 2262. Telex: 43116